BUZZ POLLINATION: INVESTIGATIONS OF POLLEN EXPULSION USING THE DISCRETE ELEMENT METHOD

by

Caelen Gallatin Boucher-Bergstedt

A thesis submitted in partial fulfillment
of the requirements for the degree

of

Master of Science

in

Mechanical Engineering

MONTANA STATE UNIVERSITY
Bozeman, Montana

May 2025

DEDICATION

Above all, my family has made me who I am. Their unwavering support, generosity, and encouragement have shaped my journey and made this work possible.

To Barbara Peterson, who inspired me to pursue my master's degree and nurtured my curiosity from an early age. Though we haven't often spoken about it, your path—from research at NASA to teaching chemistry—left a deep impression on me as a child. It helped shape how I think about perseverance, curiosity, and the value of sharing knowledge with others.

To Charlie Boucher, Frances Ellman, and Tina Gordon, whose encouragement and support enabled me to focus fully on my studies. Your generosity created the space for me to learn and grow without distraction, and your belief in my potential helped carry me forward.

To my parents, Connie Boucher and Craig Bergstedt—to whom I owe everything. You have always been there when I needed you, providing steadfast support and care. Your encouragement has given me the strength to carry on, even in moments of doubt. You instilled in me the perseverance to keep going, and for that, I am endlessly grateful.

And to my nephew Jude—may you always stay curious. You're bright, full of potential, and I hope you never stop asking questions, exploring new ideas, and believing in what you're capable of. I believe in you.

Finally, thank you to all those who have chosen to teach, to study, and to share knowledge freely—your work quietly shapes the world we live in and makes it possible for others to grow.

ACKNOWLEDGEMENTS

This research was made possible through the support of the National Science Foundation (NSF) under grant no. CMMI-2221908. Any opinions, findings, and conclusions or recommendations expressed in this material are those of the author and do not necessarily reflect the views of the NSF.

I would like to extend my deepest gratitude to my advisor, Dr. Erick Johnson, for his guidance, patience, and support throughout this project. His expertise and mentorship have been invaluable in shaping this research and my development as a scholar.

I am also grateful to my committee members, Dr. Mark Jankauski and Dr. Lewis Cox, for their time, feedback, and insightful discussions. Their perspectives and advice have strengthened the quality and rigor of this work.

A special thank you to my lab mates, Brendan Christensen and Julian Fox, whose collaboration, discussions, and camaraderie made this journey both productive and enjoyable. Their support and willingness to exchange ideas have been instrumental in my progress.

TABLE OF CONTENTS

TABLE OF CONTENTS – CONTINUED

TABLE OF CONTENTS – CONTINUED

LIST OF TABLES

LIST OF FIGURES

LIST OF FIGURES – CONTINUED

Figure Page

LIST OF FIGURES – CONTINUED

Figure Page

NOMENCLATURE

η	Displacement amplitude
ω	Angular frequency
τ	Characteristic timescale
t	Time
$\mathbf{x}$	Particle position vector
$\mathbf{v}$	Particle velocity vector
$\mathbf{a}$	Particle acceleration vector
J	Jerk (time derivative of acceleration)
m_p	Pollen grain mass
ρ_p	Pollen grain density
R	Pollen grain radius
E	Young's modulus
ν	Poisson's ratio
G	Shear modulus
F_c	Contact force
F_g	Gravitational force
F_d	Drag force
$C_{n\ rest}$	Normal coefficient of restitution
$C_{t\ rest}$	Tangential coefficient of restitution
C_{fs}	Static friction coefficient
N	Damping force
K	Stiffness constant
$t_{1/2}$	Time required for 50% of pollen grains to be expelled
$N(t)$	Number of expelled pollen grains at time t
N_0	Initial number of pollen grains
$\dot{P}$	Pollen expulsion rate
A	Acceleration amplitude
$J_{\max}$	Maximum jerk
S_{wall}	Anther wall displacement function
v_{wall}	Anther wall velocity function
Π	Force ratio comparing gravity and contact forces
St	Stokes number

ABSTRACT

Buzz pollination is a specialized mechanism by which bees extract pollen from flowers using vibrational energy. This process is essential for the reproduction of many plant species, including economically important crops such as tomatoes and blueberries. Despite its ecological and agricultural significance, the mechanical factors governing pollen expulsion remain incompletely understood. While previous experimental studies have examined how vibration frequency and amplitude influence pollen release, they often lack the ability to resolve the detailed interactions between pollen grains. This study addresses this gap by using the Discrete Element Method (DEM) to simulate pollen expulsion under vibratory excitation, providing a computational approach to analyzing pollen motion at a granular level.

Two primary simulations were conducted to model pollen expulsion: translating anther motion, in which the entire anther oscillates as a rigid body, and deforming anther motion, which accounts for structural vibrations that more closely resemble natural conditions. In the translating anther simulations, pollen-pollen interactions played a critical role in directing grains toward the anther pore, challenging prior assumptions that grains move independently. Initial analyses of total pollen expulsion over long time periods showed little variation across different vibration settings. However, by examining earlier time steps, trends emerged that revealed higher displacement amplitudes and frequencies led to more rapid pollen release. To quantify this effect, expulsion rates were measured based on the time required to eject half of the initial pollen grains. These results were further analyzed using a parameter called jerk, which describes how rapidly acceleration changes over time. Jerk was found to be a strong predictor of pollen expulsion rates, effectively collapsing the parameter space into a single governing variable.

Simulations of deforming anthers introduced additional complexity, as the shape and motion of the anther influenced the efficiency of pollen release. The findings suggest that vibratory forces are distributed differently in deforming anthers compared to rigidly translating ones, leading to differences in expulsion behavior. This study advances the understanding of vibratory pollen expulsion mechanics and provides a foundation for future research into artificial pollination technologies and pollination efficiency in natural ecosystems.

INTRODUCTION

Buzz pollination, a biomechanical process critical to the reproduction of many flowering plants, plays a pivotal role in sustaining global biodiversity and agricultural productivity. This unique phenomenon involves pollinators, primarily bees, using rapid muscle contractions to generate vibrations that release pollen from specialized floral structures known as poricidal anthers [5]. These vibrations facilitate efficient pollen transfer, ensuring fertilization in plant species that rely on this mechanism.

Given its importance in both natural ecosystems and agricultural settings, understanding the mechanics of buzz pollination is essential for preserving pollinator populations and enhancing crop yields. This chapter provides a comprehensive overview of buzz pollination, beginning with its ecological and economic significance. It then explores the historical context of research on the topic, highlighting key discoveries. Additionally, it addresses experimental challenges that have motivated the use of computational models to study pollen expulsion. Finally, the chapter outlines the objectives and scope of this thesis, setting the foundation for subsequent analyses and contributions.

The Importance of Buzz Pollination

Buzz pollination, also known as sonication (a misnomer due to the sound produced by buzzing bees), is a unique and essential pollination mechanism employed by certain pollinators to release pollen from flowers with, primarily, poricidal anthers. These anthers, characterized by small apical pores or slits, require this more complex form of pollination to eject pollen due to their secure form of pollen retention. Unlike anthers that passively shed pollen into the air or onto visiting insects, poricidal anthers hold pollen tightly within

locules, necessitating external vibrations to force pollen release.

This specialized mechanism ensures targeted pollen transfer and reduces pollen wastage, making it an adaptive advantage for both plants and pollinators [15]. Many bee species, particularly bumblebees (*Bombus spp.*), have evolved the ability to produce vibrations using their indirect flight muscles, a process that extracts pollen from these specialized anthers [7]. Some solitary bees, such as those in the genera *Xylocopa* and *Ceratina*, also engage in buzz pollination, broadening the ecological impact of this process [6].

Buzz pollination plays a critical role in the reproduction of approximately 9–10% of all flowering plant species [6, 28, 35] and contributes to the global food supply by supporting the pollination of key crops such as tomatoes, eggplants, and kiwis [9, 11, 28]. Many of these crops are self-incompatible or exhibit increased fruit set when buzz-pollinated, underscoring the necessity of this mechanism for maximizing reproductive success [2].

Pollinator declines pose a significant threat to agricultural productivity. Without animal pollinators, global food production would face a 5–8% reduction [1, 24], necessitating the conversion of vast areas of land into agricultural use of pollinator-independent crops to compensate for yield losses [24]. However, such shifts would not fully offset the nutritional impact, as pollinator-dependent crops provide essential micronutrients, including vitamins A and C, calcium, and folic acid, that are critical for human health [24]. Beyond quantitative reductions, pollinator loss would lead to decreased quality in approximately 75% of pollinator-dependent crops, directly impacting the stability of global food markets and exacerbating food insecurity, especially in regions highly dependent on pollinator-supported agriculture [2, 24]. Furthermore, pollination-dependent crops, such as fruits, nuts, and high-value commodities like coffee and cocoa, experience lower yield growth and greater variability over time, amplifying economic and food security risks [24].

Buzz pollination is particularly vital in these contexts, as many of the crops reliant on this mechanism, such as tomatoes, blueberries, eggplants, kiwis, and cranberries, are

staples in various diets and have high economic value [2]. The efficiency of pollen transfer associated with this process enhances genetic diversity and improves fruit set (the transition of a flower to a young fruit) and seed quality, contributing to the long-term resilience of plant populations [2]. However, agricultural intensification, habitat fragmentation, and pesticide exposure threaten native bee species capable of buzz pollination, reducing their availability as effective pollinators [24]. Given that wild pollinators often provide more stable pollination services than managed honeybees [2], their conservation is essential for sustaining both crop productivity and ecosystem health.

Agricultural and Economic Significance

Studies have demonstrated that natural pollination enhances crop yields and quality compared to artificial pollination techniques [2]. Crops exhibit higher fruit set, improved fruit quality, and increased seed viability when pollinated by buzzing bees, highlighting the evolutionary advantage of this specialized pollination mechanism [9]. For instance, research on tomatoes (*Solanum lycopersicum L.*) showed that fruit weight more than doubled when buzz-pollinated by bees compared to artificially pollinated plants [8]. This suggests that natural pollination processes not only meet but exceed the effectiveness of current human interventions, emphasizing the critical role of buzz pollination in sustainable agriculture. Beyond tomatoes, buzz pollination is essential for a range of economically important crops, including blueberries (*Vaccinium spp.*), cranberries (*Vaccinium macrocarpon*), eggplants (*Solanum melongena*), kiwis (*Actinidia spp.*), and peppers (*Capsicum spp.*) [35].

The decline of wild pollinator populations poses a direct threat to the agricultural industries dependent on buzz pollination. Studies indicate that reduced bee populations could lead to a significant decrease in fruit set and crop viability, particularly in regions where managed honeybees (*Apis mellifera*) are ineffective substitutes due to their inability to perform buzz pollination [2]. Farmers in some regions have resorted to costly artificial

pollination techniques, such as using electric vibrators or manual agitation of flowers, but these methods are labor-intensive and often fail to replicate the efficiency of natural pollination. Countries like Japan and Australia, where greenhouse tomato production is extensive, have explored commercial bumblebee rearing programs to mitigate this issue [16, 26].

The economic significance of buzz-pollinated crops extends beyond direct agricultural revenue. Increased reliance on artificial pollination could drive up production costs, potentially raising consumer prices for staple fruits and vegetables. Additionally, the loss of buzz-pollinating bees could disrupt agricultural supply chains that depend on pollination services.

However, natural buzz pollinators face increasing threats from habitat fragmentation, pesticide exposure, and climate change, leading to declining populations in many regions [24, 32]. While conservation efforts aim to mitigate these declines, their long-term success remains uncertain. Without effective conservation, an improved understanding of the mechanics of buzz pollination is essential for developing alternative strategies to sustain crop productivity and minimize economic risks associated with pollinator loss.

From an economic perspective, buzz-pollinated crops constitute a substantial portion of agricultural revenue. The contribution of pollination services, including buzz pollination, is estimated to add billions of dollars annually to global agricultural economies [2, 24]. The economic impact of pollination extends beyond direct crop value, supporting approximately 1.4 billion agricultural workers worldwide. In developing nations, over 2 billion people rely on smallholder farming, which is particularly dependent on pollinators [24]. However, declining pollinator populations could drive up food prices, potentially reducing consumer welfare by an estimated $160–191 billion annually [24].

Ecological Significance

Beyond its economic role, buzz pollination plays a critical part in maintaining biodiversity and ecosystem stability. One of the most significant ecological benefits of buzz pollination is its role in promoting genetic diversity within plant populations. Many buzz-pollinated species exhibit self-incompatibility mechanisms, requiring pollen transfer between different individuals for successful fertilization [2, 14]. This process enhances genetic variation, which is crucial for plant adaptability to environmental changes such as shifting temperatures, altered precipitation patterns, and the introduction of new pests and diseases [9]. Greater genetic diversity strengthens plant populations against environmental stressors and contributes to the long-term resilience of ecosystems.

Buzz pollination also supports plant-pollinator networks by enabling the reproduction of plants that provide essential food and habitat for other organisms. Many wildflowers, shrubs, and trees that rely on buzz pollination serve as keystone species in their ecosystems, sustaining insect populations, birds, and herbivores. The decline of these plants due to reduced pollination rates can lead to cascading effects across entire food webs, threatening ecosystem stability. However, the introduction of non-native bumblebee species for agricultural pollination, such as *Bombus terrestris* in Japan and Tasmania, has raised ecological concerns. These introduced bees may compete with native pollinators for floral resources, potentially leading to the displacement of indigenous species and alterations in plant-pollinator interactions [16, 26]. In Japan, *B. terrestris* has been linked to reduced biodiversity in certain pollinator communities, prompting regulatory measures to limit its spread. Australia, recognizing these risks, has implemented strict biosecurity laws preventing bumblebee introductions on the mainland [16, 26].

The primary threats to buzz pollination arise from habitat destruction, pesticide use, and climate change. Deforestation and agricultural intensification have significantly reduced the availability of nesting sites and floral resources for native pollinators [38]. Pesticides,

particularly neonicotinoids, have been shown to impair the foraging efficiency of buzz-pollinating bees, reducing their ability to effectively pollinate flowers [29]. Furthermore, pesticide effects on bees are temperature-dependent, with some impacts exacerbated by higher temperatures, which is an increasing concern given global climate change [29]. Rising global temperatures and shifting climate patterns may alter the geographic distribution of both plants and pollinators, disrupting long-established pollination relationships and leading to potential species mismatches [19]. Climate-driven range shifts have been observed in bumblebee populations, with species failing to expand their ranges northward while experiencing significant contractions at their southern range limits [19].

The loss of buzz-pollinating bee species could have irreversible consequences for biodiversity. Studies have shown that specialized pollinators, including many buzz-pollinating bees, are at higher risk of extinction compared to generalist species due to their dependence on specific plant groups [32]. If key pollinators are lost, many plants that rely exclusively on buzz pollination may face population declines or extinction, leading to further disruptions in ecosystem function. The introduction of managed bumblebees for greenhouse pollination further complicates conservation efforts, as the risk of disease transmission to wild pollinators remains a significant concern [16, 26].

Addressing these ecological challenges requires conservation strategies that protect native pollinators and their habitats. Efforts such as pollinator-friendly land management, reduced pesticide usage, and climate-adaptive conservation planning can help preserve the critical role of buzz pollination in maintaining both species diversity and ecosystem resilience. Additionally, balancing the economic benefits of commercial pollination with ecological safeguards remains a key policy challenge, as seen in the ongoing regulatory debates surrounding bumblebee imports and trade restrictions in countries like Japan and Australia [16, 26].

Historical Context of Buzz Pollination

Early Observations & Discoveries

The earliest unambiguous records of vibratory pollen collection date back to Lindman (1902), who documented bumblebees vibrating the flowers of *Senna alata* (candle bush) in Brazil. He described the distinctive buzzing sound produced during pollen extraction and noted that the vibrations caused pollen to be forcibly expelled from the anthers [33]. Schrottky (1908) later expanded on these observations by recording vibratory pollen collection in multiple species, including *Senna occidentalis* (coffee senna), *Physalis viscosa* (sticky groundcherry), and *Solanum paniculatum* (jurubeba). His work confirmed that bees did not rely on scraping or mandible manipulation to extract pollen but rather generated vibrations that dislodged the grains from inside the anther pores [33].

Early theories on pollen extraction proposed mechanisms other than vibration. Todd (1882) suggested that bees extracted pollen using a "milking motion," in which they gripped anthers with their mandibles and squeezed out pollen through terminal pores [33]. Robertson (1890) later observed bumblebees exhibiting similar behavior on *Chamaecrista fasciculata* and *Senna marilandica*, reinforcing this interpretation [33]. The idea remained influential, with Knuth (1904) describing "milking" in the context of feeding anthers in certain *Cassia* species, though this process was unrelated to pollen release [33]. However, Schrottky (1908) directly refuted the "milking hypothesis" after observing that visiting bees did not squeeze anthers but instead generated strong vibrations to dislodge pollen grains from anther pores [33].

As additional reports accumulated, it became increasingly evident that mechanical vibrations—not mandibular manipulation—were responsible for pollen release. However, due to the lack of high-speed imaging or vibration analysis tools at the time, early researchers were unable to quantify the precise forces involved. These foundational studies set the

stage for the more systematic, laboratory-based investigations that emerged in the mid-20th century.

Scientific Investigations Over Time

The mid-to-late 20th century marked a turning point in buzz pollination research, as scientists transitioned from field-based naturalist observations to controlled laboratory experiments. By the late 1970s to mid-1990s, researchers began using high-speed photography, vibration sensors, and artificial pollination devices to systematically study the frequencies and amplitudes of bee-generated vibrations [7, 9]. These studies allowed for precise measurements of pollination dynamics, revealing that most buzz-pollinating bees produce vibrations between 100–400 Hz, frequencies often aligning with the natural resonant frequencies of anthers [33].

One of the most influential studies during this period was conducted by Buchmann and Hurley (1978), who combined laboratory experimentation with theoretical modeling to analyze vibrational pollen release [7]. Their experiments focused on mechanically vibrating *Solanum* flowers under vacuum conditions to test whether airflow played a role in pollen expulsion. By eliminating air currents, they demonstrated that pollen clouds formed in vacuum were nearly identical to those observed under normal atmospheric conditions, confirming that airflow was not a significant factor in pollen release. Additionally, they quantified pollen expulsion rates under varying vibration frequencies and amplitudes, showing that while pollen release increased with vibration intensity, it plateaued beyond a certain threshold. These findings provided strong experimental evidence that mechanical vibrations alone were responsible for pollen expulsion, disproving earlier hypotheses that relied on airflow or electrostatic forces as primary mechanisms.

Alongside their experimental work, Buchmann and Hurley developed a statistical mechanics model to describe pollen expulsion as an energy-driven process, in which pollen

grains gain kinetic energy through anther vibrations until reaching a velocity sufficient for expulsion through the anther pores. This theoretical framework will be revisited in a later section, where it is examined alongside subsequent computational models of buzz pollination. Their combined experimental and theoretical approach laid the foundation for modern biomechanical studies of vibratory pollen release, influencing future research on the mechanics of buzz pollination.

Building upon this work, Buchmann (1985) extended investigations into how bees utilize vibration beyond poricidal anthers, demonstrating that certain bee species employ similar mechanisms to extract pollen from non-poricidal flowers [6]. This broadened the scope of buzz pollination studies, revealing that vibratory pollen collection is not limited to species with specialized anther structures but is also utilized in a wider range of pollination systems. While it is intriguing to consider the reasons for bees to buzz on non-poricidal anthers, this is beyond the scope of this thesis.

Further advancements emerged in the late 1980s and early 1990s. Harder and Thomson (1989) developed a conceptual model describing how pollen release strategies optimize reproductive success in animal-pollinated plants [15]. Their work emphasized that poricidal anthers function as controlled dispensing mechanisms, regulating pollen removal across multiple pollinator visits. This idea was supported by subsequent research by Harder and Barclay (1994), who experimentally demonstrated that controlled pollen release enhances pollination efficiency by minimizing pollen wastage and maximizing pollen transfer to stigmas [14]. Their findings contributed to the broader understanding of how floral traits and pollinator behavior co-evolve to optimize reproductive success.

Experimental studies in the late 20th century focused on quantifying the relationship between vibration parameters and pollen ejection efficiency. Researchers examined how vibration frequency and amplitude influenced pollen expulsion, with studies demonstrating that pollen release generally increased with vibration amplitude but showed a more complex

relationship with frequency [14]. For instance, Harder and Barclay (1994) found that while pollen removal increased with vibration amplitude, higher frequencies did not always lead to greater pollen expulsion unless paired with sufficient displacement [14]. Similarly, Corbet (2014) reviewed multiple studies showing that pollen release depends more on vibration velocity than frequency alone, emphasizing the interaction between these parameters [9]. These experiments laid the foundation for further investigations into the biomechanics of buzz pollination.

By the 2010s, researchers had begun integrating computational modeling into buzz pollination studies, using numerical simulations to characterize pollen expulsion under different vibrational conditions [13]. This marked the transition from experimental-only studies to hybrid experimental-computational approaches, significantly expanding the scope of research in pollination biomechanics.

As scientific investigations evolved, researchers also started exploring species-specific adaptations in buzz pollination. Studies comparing the vibration characteristics of different bee species revealed that some pollinators are more effective at extracting pollen due to differences in their buzzing frequencies and muscle contraction patterns [9]. These findings contributed to broader discussions on plant-pollinator co-evolution, reinforcing the idea that buzz pollination is an adaptive strategy shaped by millions of years of ecological interactions.

Challenges in Studying Buzz Pollination

Understanding the mechanics of buzz pollination presents significant challenges due to the interplay of biological, mechanical, and observational factors. Despite decades of research, many aspects of pollen expulsion dynamics remain poorly understood, largely due to the technical limitations of experimental methods. The small scale, high-speed motion, and opacity of anther walls complicate direct observation, while experimental limitations hinder the decoupling of vibration parameters such as amplitude and frequency.

These obstacles have necessitated the development of computational models to complement experimental findings and provide deeper insights into pollen dynamics.

Experimental Challenges

Difficulties in Observing Pollen Movement Inside Anthers One of the primary challenges in studying buzz pollination is directly observing pollen movement inside the anther locules. Unlike wind or insect-pollinated flowers that open to expose pollen, poricidal anthers keep their pollen sealed within and only release it through small apical pores. This makes it impossible to visually track pollen movement in real time prior to release without sophisticated imaging techniques.

Conventional light microscopy and high-speed cameras may be sufficient for capturing the dynamics of microscopic (˜10–100 μm diameter) pollen grains after expulsion, but have yet to be used extensively. Even advanced techniques like X-ray microtomography have limitations in tracking pollen grains inside the anther as they are not capable of reaching the necessary time resolution to produce relevant results.

Some researchers have attempted to overcome these challenges by indirectly inferring pollen motion through measurements of pollen cloud dispersion [7, 27]. However, these methods only provide macro-scale insights and fail to resolve particle-scale interactions within the anther itself.

Challenges in Isolating Vibration Parameters Another major experimental difficulty lies in the decoupling of amplitude and frequency effects in pollen expulsion. In natural buzz pollination, bees generate vibrations by contracting their indirect flight muscles, which produce simultaneous changes in both frequency and amplitude. However, these two variables are often intertwined, making it difficult to determine their independent contributions to pollen release efficiency.

There is experimental evidence suggesting that the specific contributions of frequency and amplitude are difficult to isolate due to how they interact in real systems. While parameter sweeps could theoretically determine these effects, studies have shown that pollen release efficiency does not always increase linearly with vibration parameters. For example, Harder & Barclay (1994) demonstrated that controlled pollen removal from Dodecatheon flowers was optimized at certain frequencies and amplitudes, but no universal "best" parameter existed across all conditions [14]. Similarly, Rosi-Denadai et al. (2020) did not observe a clear resonant response that significantly improved pollen release [27].

Electromagnetic vibration tables and piezoelectric actuators have enabled more precise control over amplitude and frequency, but these methods still face limitations. For example, many artificially vibrated anthers do not exhibit the same flexural deformations as those vibrated by bees, raising concerns about the validity of lab-based pollen expulsion studies. Furthermore, Jankauski et al. (2022) suggested through computational modeling that resonant frequencies may align with reported buzzing frequencies, but only when the bee's mass was included in the model [17]. This suggests that real-world dynamics introduce complexities that cannot be fully captured through simple parameter sweeps.

Thus, while a parameter sweep might theoretically determine independent contributions of frequency and amplitude, real-world interactions between bee physiology, anther deformation, and pollen behavior complicate straightforward conclusions. These experimental limitations underscore the need for integrated experimental-computational approaches, where high-resolution simulations can supplement physical experiments and help deconvolve the relative effects of frequency, amplitude, and anther morphology on pollen expulsion dynamics.

Knowledge Gaps

Despite the advancements in experimental methods, several critical questions about the mechanics of buzz pollination remain unresolved. Many of these knowledge gaps stem from the limitations of current measurement techniques, which make it difficult to directly observe pollen behavior inside anthers and quantify the forces governing its ejection.

Unresolved Questions About Pollen-Anther Interactions One of the most pressing unknowns in the computational study of buzz pollination is how pollen grains interact with the anther walls and with each other during vibration. Many existing models assume that pollen grains behave independently, neglecting potential effects such as inter-particle collisions, clustering, and triboelectric interactions. However, real anther locules contain thousands of pollen grains, which likely experience frequent interactions that influence their motion and expulsion .

The role of pollen-anther interactions in buzz pollination has been explored through various approaches, including biophysical modeling and experimental studies. Buchmann and Hurley [7] developed a biophysical model demonstrating that pollen grains gain kinetic energy through repeated collisions with anther walls, ultimately facilitating their expulsion. Additionally, triboelectric charging, arising from pollen grain collisions with anther surfaces, has been hypothesized to contribute to pollen ejection [9]. Experimental and modeling work suggests that ignoring these interactions in computational studies could lead to an oversimplified representation of pollen expulsion dynamics.

The mechanical properties of anther walls remain another unresolved factor in pollen release. Some studies suggest that anthers may undergo elastic deformations during vibration, potentially influencing the pollen expulsion behavior [17]. However, direct measurements of anther flexural properties under natural pollination conditions remain scarce, leaving researchers to approximate these effects using indirect methods [14]. Understanding the role

of anther wall dynamics is crucial, as variations in stiffness and elasticity could significantly impact pollen release.

Addressing these gaps is critical for improving computational approaches to buzz pollination. By incorporating detailed models of pollen-anther interactions, including energy transfer, electrostatic effects, and anther deformation, researchers can develop simulations that better reflect the complexities observed in experimental studies.

The Need for Quantitative Methods to Measure Pollen Expulsion A major limitation in buzz pollination studies is the lack of standardized quantitative methods for assessing pollen expulsion. Most experiments rely on qualitative or semi-quantitative assessments, such as:

- Counting the total number of expelled pollen grains,
- Measuring pollen cloud dispersion patterns, or
- Estimating pollen deposition on stigmas.

However, these approaches fail to capture the fine-scale physics of pollen motion. For example, studies often assume that higher vibration intensity leads to greater pollen release, yet the relationship between vibration forces and pollen ejection is not fully understood. Some research, such as that seen in Harder and Barclay [14], has demonstrated that pollen is expelled in discrete doses rather than continuously, with each vibration event releasing a limited amount of pollen. While these findings provide valuable insight into pollen expulsion dynamics, existing experimental methods still lack the temporal resolution needed to fully resolve the mechanisms governing burst-like pollen release at the millisecond scale.

To address these gaps, researchers are now leveraging numerical simulations that model pollen dynamics at the micron scale that will support ongoing experimental work.

Computational Approaches to Buzz Pollination

Computational models have emerged as tools to supplement experimental findings, enabling controlled parameter variation, high-resolution insights, and systematic analysis of pollen expulsion dynamics. Several numerical approaches have been developed to characterize pollen motion under vibrational forces, including statistical mechanics models, billiard-based models, and the discrete element method (DEM). Each of these models provides a unique perspective on pollen expulsion, but they also have limitations in capturing all aspects of the process.

This section outlines the development of computational approaches for studying buzz pollination, summarizing prior models and their constraints before introducing DEM as a powerful tool for simulating pollen-pollen interactions and anther deformations. The mathematical formulation and implementation details of DEM are further discussed in Chapter 2.

The Need for Computational Modeling

Computational modeling addresses challenges faced by experimental methods by allowing researchers to systematically control variables that are difficult to manipulate experimentally. By simulating high-speed pollen motion in a controlled virtual environment, models can provide detailed insights into pollen-pollen interactions and the influence of anther morphology. These approaches make it possible to explore a wide range of conditions, in a controlled and infinitely repeatable manner, including different vibration parameters and anther geometries, to better understand the factors that optimize pollen expulsion.

Overview of Prior Models

Theoretical models for pollen expulsion in buzz pollination have evolved considerably over the past several decades. Initial approaches relied on statistical mechanics principles,

treating pollen motion as an energy transfer problem, while later studies applied billiard-based models to simulate pollen trajectories. Although these models have contributed significantly to the field, they often relied on simplifying assumptions that limited their ability to fully capture the complexities of vibratory pollen release.

Statistical Mechanics Model One of the earliest quantitative models of buzz pollination was the statistical mechanics framework proposed by Buchmann and Hurley in 1978. This model conceptualized the anther as a rectangular cavity containing thousands of pollen grains, which gain kinetic energy through externally applied vibrations. The model assumed that pollen grains follow a Maxwell-Boltzmann energy distribution, with anther walls transferring kinetic energy to grains through oscillatory motion. Pollen was predicted to exit through the apical pore when it acquired sufficient velocity [7].

Rather than modeling individual pollen-pollen interactions explicitly, the model accounts for their collective behavior by treating the total system energy statistically. This approach prevents pollen grains from immediately reaching maximum energy, as energy is distributed throughout the system rather than instantaneously imparted to all particles. However, the model does not account for detailed per-particle interactions such as clustering, adhesion, or triboelectric effects. Additionally, it assumes that grains behave as idealized particles and does not include potential cohesion forces or anther flexibility that might influence their motion.

Hansen's Billiards Model A more recent approach by Hansen and colleagues (2021) applied billiards theory to describe pollen release under vibratory excitation. In this model, pollen grains were treated as inelastic particles undergoing repeated collisions within an oscillating anther chamber. The results indicated that peak anther velocity played a more significant role in pollen expulsion than vibration frequency alone. However, both vibration amplitude and frequency contribute to mechanical energy transfer, influencing the kinetic

energy gained by pollen grains [13].

Despite its improvements over earlier models, the billiards approach still relied on several simplifications. Pollen grains were treated as non-cohesive particles, meaning that interactions such as adhesion and electrostatic forces were not considered. Particles were also assumed to be non-interacting due to a small volume fraction. Additionally, while the model was formulated to allow for modifications, it was evaluated with $c = 1$. The model also initialized pollen grains with a nonzero velocity, rather than assuming they were initially at rest. These factors can significantly influence pollen aggregation and dispersal, particularly in species where pollen clumping may affect expulsion.

The Discrete Element Method

To overcome the limitations of previous models, the discrete element method (DEM) has been applied to study granular systems [12] and is used in this work for investigating buzz pollination. DEM is a numerical approach that simulates the motion and interactions of individual particles under external forces, making it well-suited for modeling the vibratory behavior of pollen grains inside an anther.

Unlike prior models, the proposed DEM model explicitly accounts for pollen-pollen interactions and has the ability to include easily collisions, cohesion, and electrostatic forces, as well as boundary effects imposed by anther walls in the future. By incorporating realistic material properties, DEM can simulate how anther deformations influence pollen expulsion, making it a powerful tool for investigating the mechanics of buzz pollination.

Application of DEM in This Research While experimental methods provide valuable insights into buzz pollination, they face limitations in resolving fine-scale pollen dynamics. DEM fills these gaps by enabling simulations that track thousands of pollen grains in ways that would be impractical in laboratory settings. It allows researchers to explore a wide range of anther geometries, vibration parameters, and pollen properties under controlled

conditions, offering a complementary approach to experimental studies.

A key strength of DEM is its ability to incorporate adhesion and elasticity, providing a framework for investigating how cohesive forces affect pollen expulsion . This is particularly important in species where pollen grains exhibit strong inter-particle forces, which can alter the timing and quantity of expelled pollen. By integrating these factors, DEM serves as a bridge between mechanical modeling and real-world mechanics, offering predictions that can guide and refine experimental studies.

This thesis extends the use of DEM into buzz pollination research by applying it to simulate pollen expulsion under realistic vibration conditions, and more. The approach includes modeling anther vibrations based on experimentally observed frequencies and amplitudes, examining how different anther geometries affect pollen expulsion, and evaluating the role of material properties such as pollen restitution. By systematically varying these parameters, DEM enables a comprehensive analysis of the factors influencing pollen expulsion .

The computational methods described in this section provide the foundation for the numerical framework developed in this study. Chapter 2 presents a detailed discussion of the DEM implementation, including the governing equations, numerical methods, and parameter selection used in the simulations.

Objectives and Scope of this Thesis

The primary objective of this thesis is to improve the understanding of pollen expulsion mechanics in buzz pollination by leveraging computational modeling. While previous studies have provided valuable insights into the role of vibration parameters in pollen release, significant gaps remain in quantifying the influence of pollen-pollen interactions, anther deformations, and material properties on expulsion . Addressing these gaps requires a computational approach capable of simulating these effects with high accuracy.

This research extends the application of the discrete element method to buzz pollination by developing a computational framework that models pollen motion under vibrational excitation. Unlike previous models, this study incorporates anther deformation effects and explicitly examines how key factors—including vibration frequency, amplitude, anther geometry, and pollen material properties—affect pollen expulsion rates. Additionally, this work quantifies the role of particle restitution in pollen release and establishes a direct relationship between the jerk of the anther wall and pollen expulsion dynamics. Finally, the computational results are compared against experimental trends, demonstrating that DEM can successfully capture key features of pollen expulsion, thereby validating its use as a modeling tool in buzz pollination research.

Beyond its contributions to fundamental research, this work has broader implications in both ecology and agriculture. The insights gained from DEM modeling can inform future experimental studies by providing testable hypotheses and quantitative predictions. Additionally, the findings may support the optimization of artificial pollination techniques for crops that rely on buzz pollination, as well as conservation strategies for pollinator-dependent plant species by improving the understanding of pollen transfer .

Thesis Structure

This thesis is structured to provide a comprehensive examination of buzz pollination mechanics, beginning with theoretical foundations and culminating in numerical results and conclusions.

- **Chapter 2: Theoretical Framework and Computational Methods** This chapter presents the governing equations, force models, and numerical implementation of DEM. It outlines the key assumptions, boundary conditions, and parameter selection used in the simulations.

- **Chapter 3: Simulation Results and Analysis** This chapter discusses the results obtained from DEM simulations, examining the effects of vibration parameters, anther geometry, and pollen material properties on expulsion behaviour.

- **Chapter 4: Conclusions** The final chapter synthesizes the findings of this research, highlighting key insights and potential applications. It also outlines directions for future work, including refinements to the computational model and experimental validations.

THEORY

This section provides an overview of the computational approach used in this thesis, specifically the Discrete Element Method (DEM) and its implementation in Siemens' SimCenter STAR-CCM+ 2206. Additionally, the specific simulations models and parameters used for this work are detailed.

Discrete Element Method (DEM)

Fundamental Principles

A useful way to visualize DEM is to imagine the opening break in a game of billiards. When the cue ball strikes the neatly racked set of balls, energy is transferred through individual collisions, causing balls to scatter, bounce off each other, and interact with the table's boundaries. Each ball follows Newton's laws of motion, moving independently based on its own velocity and the forces acting upon it. Approximated in a computer, the cue ball would impart an initial force, and subsequent interactions between balls would be calculated step by step over many hundreds to thousands of tiny fractions of a second, resolving contact forces, energy dissipation, and momentum transfer over the period of interest.

Unlike many traditional numerical modeling approaches that rely on a fixed mesh—a collection of discrete elements that subdivide a domain into smaller, well-defined pieces to solve a system of partial differential equations—DEM centers the reference frame and equations of motion on each particle [10]. This methodology is particularly useful for handling large length-scale differences, such as particles with diameters in the micron range and travel paths up to ten millimeters. Because DEM operates in a Lagrangian framework, surface and body forces are computed individually for each particle of mass m and summed to determine the total force acting on the particle. Newton's second law is then used to compute acceleration:

$$\mathbf{F_{tot}} = m\mathbf{a}. \tag{1}$$

This concept is discussed in detail in the next section, where the particle equations of motion are defined.

DEM particles are not necessarily spherical; they can have faceted shapes. However, assuming pollen grains to be smooth and spherical [21], the rotational energy in this problem is negligible. As a result, the rotational momentum balance typically considered in DEM can be ignored, and a detailed description is omitted.

From a known acceleration of a particle, integrating twice yields its position:

$$\mathbf{x} = \mathbf{x_0} + \mathbf{v}t + \mathbf{a}t^2 \tag{2}$$

With a sufficiently small time step Δt, the position $\mathbf{x}$ of each particle is updated in two stages: first, the velocity is updated as

$$\mathbf{v_{new}} = \mathbf{v_{old}} + \mathbf{a}\Delta t, \tag{3}$$

and then the position is updated as

$$\mathbf{x_{new}} = \mathbf{x_{old}} + \mathbf{v_{new}}\Delta t. \tag{4}$$

This process is repeated for all particles, for each time-step, until the simulation ends. Bold variables in these equations indicate vector quantities.

Particle Equations of Motion

Governing Equations of Motion The motion of each particle is determined primarily by surface forces and body forces, given by:

$$m_p \frac{d\mathbf{v}_p}{dt} = \mathbf{F}_s + \mathbf{F}_b, \tag{5}$$

where $\mathbf{v}_p$ is the instantaneous particle velocity, $\mathbf{F}_s$ represents the resultant surface forces acting on the particle, and $\mathbf{F}_b$ represents the resultant body forces.

The surface and body forces can be further decomposed as

$$\mathbf{F}_s = \mathbf{F}_d + \mathbf{F}_p + \mathbf{F}_{vm} \tag{6}$$

and

$$\mathbf{F}_b = \mathbf{F}_g + \mathbf{F}_{MRF} + \mathbf{F}_c + \mathbf{F}_{Co}, \tag{7}$$

where $\mathbf{F}_d$ is the drag force, $\mathbf{F}_p$ is the pressure gradient force, $\mathbf{F}_{vm}$ is the virtual mass force, $\mathbf{F}_g$ is the gravitational force, $\mathbf{F}_{MRF}$ accounts for forces acting on a particle in a rotating reference frame, $\mathbf{F}_c$ is the contact force, and $\mathbf{F}_{Co}$ is the Coulomb force.

The surface forces represent the total momentum exerted on a particle by the surrounding medium. In coupled modeling approaches, these forces—such as drag ($\mathbf{F}_d$), pressure gradients ($\mathbf{F}_p$), and virtual mass effects ($\mathbf{F}_{vm}$)—arise due to interactions between the particles and the surrounding fluid. Drag force opposes particle motion due to viscous interactions, pressure gradient forces stem from spatial variations in fluid pressure, and

virtual mass forces account for the inertia of displaced fluid when a particle accelerates through it.

While these forces may contribute to pollen dynamics, they are not included in the present DEM framework. This decision follows the approach taken in Hansen et al. [13], where fluid effects were omitted to focus on the granular mechanics of pollen expulsion. Additionally, prior experimental work by Buchmann and Hurley (1978) [7] suggested that pollen expulsion occurred similarly in vacuum conditions, implying that aerodynamic forces may not be the primary driver of pollen release.

Given these considerations, neglecting fluid forces serves as a reasonable first approximation for modeling pollen expulsion, allowing simulations to proceed without the added complexity of fluid-particle coupling. However, future studies may incorporate these effects to better capture potential secondary influences on pollen trajectories, particularly in cases where airflow within the anther could play a role.

In DEM modeling, body forces represent external forces acting on each particle due to external fields, rotational, and inter-particle interactions. These forces include the gravitational force ($\mathbf{F}_g$), forces arising from a rotating reference frame ($\mathbf{F}_{MRF}$), contact forces ($\mathbf{F}_c$), and Coulomb forces ($\mathbf{F}_{Co}$). Each of these forces contributes to the overall motion of particles in the system, with contact forces playing a particularly critical role in granular interactions.

A study by Bowker and Crenshaw [3] found an average positive charge across seven plant species of approximately 0.32 fC with values ranging from -0.6 fC to 1.2 fC depending on the species, yielding electrostatic forces that are of the same order as the gravitational force. From preliminary simulations and further justifications presented in later in this thesis, it was determined that gravitational acceleration had a negligible impact and mirrors the observations of [7] where the anther orientation did not significantly impact pollen expulsion. Although Nevard and Vallejo-Marín (2022) examined pollen deposition rather

than expulsion, they similarly found no significant effect of floral orientation on deposition across multiple *Solanum* species [22]. As such, gravity and electrostatic forces are also excluded in this initial study. Considering these simplifications, the total force acting on a pollen particle consists of only contact forces with other particles and walls. The forces arising from the ($\mathbf{F}_{MRF}$) term also fall out due to the lab reference frame used in Siemens' SimCenter STAR-CCM+ 2206.

Contact forces ($\mathbf{F}_c$) govern both particle-particle and particle-boundary interactions. These forces arise when particles come into direct contact, leading to deformation and force transmission according to a defined contact model. Contact interactions consist of both normal and tangential components, which influence the transfer of momentum and energy within the system. In this study, the Hertz-Mindlin no-slip contact model is employed to describe these interactions, providing a framework capable of calculating elastic and dissipative forces between pollen grains and anther walls. A full description of this model follows in the next section.

Since DEM particles have orientations, angular momentum must also be conserved:

$$\mathbf{I}_p \frac{d\boldsymbol{\omega}_p}{dt} = \mathbf{M}_b + \mathbf{M}_c. \tag{8}$$

However, assuming pollen grains to be smooth and spherical [21], the rotational energy in this problem is negligible. As a result, a detailed discussion of rotational dynamics is omitted.

Hertz-Mindlin Contact Modeling The Hertz-Mindlin no-slip contact model is used to compute the normal (F_n) and tangential (F_t) components of the reaction force between two colliding particles:

$$\mathbf{F}_c = F_n \hat{\mathbf{n}} + F_t \hat{\mathbf{t}}, \tag{9}$$

where the normal direction $\hat{\mathbf{n}}$ follows the line connecting the particle centers, and the tangential direction $\hat{\mathbf{t}}$ is parallel to a modified difference of the two particle velocities [12, 34]. Figure 1 provides a simplified representation of the contact force between two spheres, A and B. If multiple spheres interact simultaneously, the forces from each sphere pair are evaluated separately and then summed to obtain the cumulative contact force.

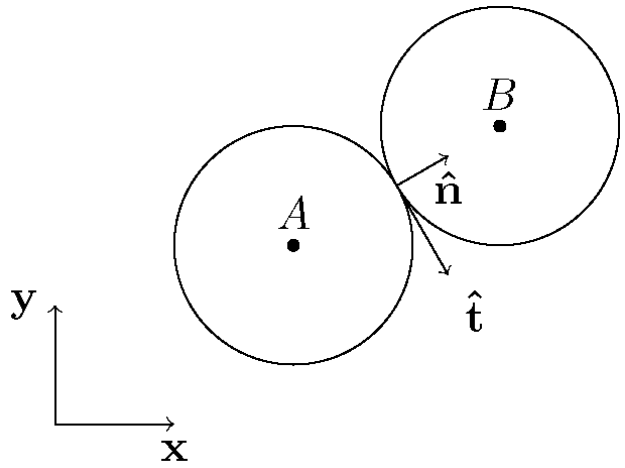

Figure 1: Simplified collision of two particles with tangential and normal force components.

The normal and tangential force components are determined using Equations 10a–10c and 11a–11c, where subscripts n and t indicate normal and tangential components, respectively. These forces incorporate the material stiffness, K, and damping, N. Stiffness quantifies the force required to stretch or compress a particle by a unit length, while damping represents the force opposing this deformation rate, scaled by the coefficient of restitution, C_{rest}. This coefficient is a dimensionless number that indicates the fraction of kinetic energy retained after a collision, where $C_{rest} = 1$ corresponds to a perfectly elastic collision, and $C_{rest} = 0$ signifies complete energy dissipation. The material damping terms vanish for perfectly elastic collisions. The tangential force is conditionally dependent on the static friction coefficient, C_{fs}.

$$F_n = -K_n d_n - N_n v_n, \tag{10a}$$

$$K_n = \frac{4}{3} E_{eq} \sqrt{d_n R_{eq}}, \tag{10b}$$

$$N_n = \frac{-\sqrt{(5 K_n M_{eq})} \ln (C_{n\ rest})}{\sqrt{\pi^2 + \ln (C_{n\ rest})^2}}. \tag{10c}$$

Due to the finite time step during a simulation, the geometry of the two particles will overlap by a small amount, d, in each direction [10], making Figure 1 an idealized depiction. The progression of particle overlap is illustrated in Figure 2.

During a collision, the relative velocity, $\boldsymbol{v}$, between two particles plays a critical role in determining the interaction forces. This velocity is decomposed into normal and tangential components, which define how momentum is transferred between the contacting particles. The normal component of velocity contributes to compression and restitution, influencing the extent of overlap and subsequent separation after impact. Meanwhile, the tangential component governs the sliding or rolling motion at the contact point, contributing to frictional forces. These decompositions are fundamental to the Hertz-Mindlin contact model, as they allow for the independent treatment of normal and tangential forces during particle collisions. The forces governing these interactions are expressed in Equations 10 and 11.

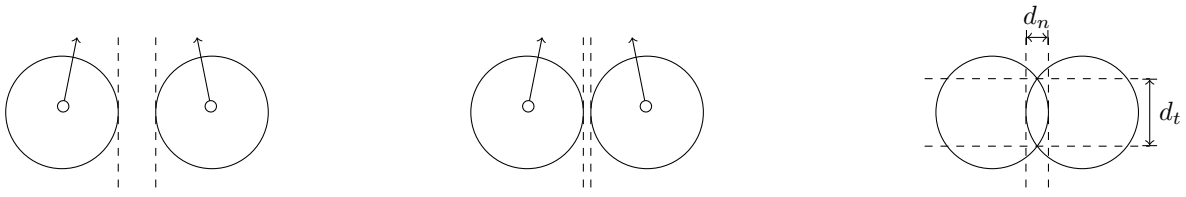

Figure 2: Progression of two colliding particles and their resulting overlap. In (a) ($t = t_0$), the particles begin their trajectories separated. In (b) ($t = t_0 + \Delta t$), the particles are near collision but remain separated, with time stepping proceeding along their original trajectories. In (c) ($t = t_0 + 2\Delta t$), the particles have collided, resulting in a registered overlap.

$$F_t = \begin{cases} \frac{|K_n d_n| C_{fs} d_t}{|d_t|}, & |K_t d_t| < |K_n d_n| C_{fs}, \\ -K_t d_t - N_t v_t, & \text{otherwise.} \end{cases} \tag{11a}$$

$$K_t = 8 G_{eq} \sqrt{d_n R_{eq}}, \tag{11b}$$

$$N_t = \frac{-\sqrt{(5 K_t M_{eq})} \ln (C_{t\ rest})}{\sqrt{\pi^2 + \ln (C_{t\ rest})^2}}. \tag{11c}$$

Equations 10 and 11 utilize equivalent physical values, defined as

$$M_{eq} = \frac{1}{\frac{1}{M_A} + \frac{1}{M_B}}, \tag{12a}$$

$$R_{eq} = \frac{1}{\frac{1}{R_A} + \frac{1}{R_B}}, \tag{12b}$$

$$E_{eq} = \frac{1}{\frac{1-\nu_A^2}{E_A} + \frac{1-\nu_B^2}{E_B}}, \tag{12c}$$

$$G_{eq} = \frac{1}{\frac{2(2-\nu_A)(1+\nu_A)}{E_A} + \frac{2(2-\nu_B)(1+\nu_B)}{E_B}}, \tag{12d}$$

where spheres A and B may have distinct masses M, radii R, and material properties. Here, E is the Young's modulus, and ν is the Poisson's ratio. The shear modulus G is computed from these parameters. When applying the Hertz-Mindlin no-slip contact model to a sphere-wall interaction, the wall is assumed to have infinite radius and mass, i.e., $R_{wall} = \infty$ and $M_{wall} = \infty$.

The Hertz-Mindlin no-slip contact model was selected for its ability to capture both normal and tangential forces during particle collisions, making it a widely used approach in DEM simulations. Unlike simpler linear spring-dashpot models, it accounts for the nonlinear stiffness of elastic contacts, which is particularly relevant for pollen grains undergoing repeated, high-frequency interactions. While pollen grains are not rigid like traditional DEM materials such as sand or gravel, the Hertz-Mindlin model remains a reasonable choice because it effectively captures nonlinear elastic behavior. This provides a foundation for future refinements that could incorporate additional pollen-specific properties, such as particle compliance, triboelectric charging, or viscoelastic effects. By using this model, we establish a baseline representation of pollen expulsion dynamics while ensuring flexibility for more detailed studies in the future.

Scaling Considerations and Non-Dimensional Analysis Understanding the relative importance of different forces acting on pollen grains is useful for validating key modeling assumptions in DEM. By employing non-dimensional parameters, we systematically assess whether forces such as fluid drag and gravity play a significant role in pollen motion or if they can be reasonably neglected. This approach provides a quantitative basis for simplifying the governing equations while ensuring that the primary drivers of pollen expulsion—contact forces and anther vibrations—are accurately captured. Additionally, these scaling arguments offer insight into conditions under which fluid or gravitational effects may become relevant,

guiding potential extensions of this work. In particular, the Stokes number (St) determines whether fluid forces significantly affect pollen movement, while the force ratio (Π) provides insight into the role of gravity relative to contact interactions.

To assess the relative importance of fluid forces on pollen motion, we estimate the Stokes number, which is defined as:

$$St = \frac{\rho_p d_p v}{9\mu}, \tag{13}$$

where ρ_p is the pollen density, d_p is the pollen diameter, v is the characteristic pollen velocity, and μ is the dynamic viscosity of air.

Representative values from Table 1 are used for this analysis ($\rho_p = 1000$ kg/m^3, $d_p = 1.0 \times 10^{-5}$ m, and $\mu = 1.8 \times 10^{-5}$ Pa·s). The velocity v is estimated based on the anther wall movement ($v \approx 0.1$ m/s) and serves as an approximation for characterizing the relative influence of fluid forces on pollen motion. This value is lower than the peak tip velocity observed in deforming anthers by [20], but provides a reasonable basis for evaluating the Stokes number. The Stokes number is then estimated as:

$$St \approx 6.2. \tag{14}$$

Since $St > 1$, the inertia of pollen grains dominates over fluid drag, indicating that particles do not significantly follow airflow but instead move primarily due to contact interactions and anther vibrations. This justifies the assumption that fluid effects can be neglected in the DEM simulations, meaning we can remove the entirety of the aerodynamic term $\mathbf{F}_s$ term from Eq. 5.

Although air resistance may influence pollen motion, the characteristic ejection speeds

observed in vibrational pollen release experiments suggest that direct particle collisions are the dominant force driving expulsion. This analysis indicates that fluid interactions are secondary in the present simulations; however, for cases where $St \approx 1$ or lower, future studies may benefit from incorporating fluid coupling effects to fully capture pollen dynamics.

To assess the relative influence of gravitational forces compared to contact forces in pollen motion, we define the force ratio Π as:

$$\Pi = \frac{F_g}{F_c} = \frac{m_p g}{K_n d_n}, \tag{15}$$

where $F_g = m_p g$ is the gravitational force on a pollen grain, K_n is the normal contact stiffness, and d_n is the characteristic deformation of the pollen grain during contact. A small value of Π ($\Pi \ll 1$) indicates that contact forces dominate over gravitational forces, implying that particle motion is driven primarily by anther vibrations and inter-particle interactions rather than settling under gravity.

The normal contact deformation d_n can be estimated by considering the kinetic energy of a pollen grain during a collision with a rigid wall. The deformation can be approximated by equating the initial kinetic energy to the elastic potential energy stored in the contact:

$$\frac{1}{2} m_p v^2 = \frac{1}{2} K_n d_n^2. \tag{16}$$

Solving for d_n:

$$d_n = \sqrt{\frac{m_p v^2}{K_n}}. \tag{17}$$

Using representative values from Table 1, where $m_p = 4.2 \times 10^{-10}$ kg, $K_n = 1.6 \times 10^9$ N/m, and assuming a characteristic velocity of $v \approx 0.1$ m/s (derived from anther wall velocities observed in [20]), we obtain:

$$d_n = \sqrt{\frac{(4.2 \times 10^{-10}\ \text{kg})(0.1\ \text{m/s})^2}{1.6 \times 10^9\ \text{N/m}}}. \tag{18}$$

$$d_n \approx 1.6 \times 10^{-8}\ \text{m} = 16\ \text{nm}. \tag{19}$$

Substituting this value into Eq. 15, using $g = 9.81$ m/s^2, we obtain:

$$\Pi = \frac{(4.2 \times 10^{-10}\ \text{kg})(9.81\ \text{m/s}^2)}{(1.6 \times 10^9\ \text{N/m})(1.6 \times 10^{-8}\ \text{m})}. \tag{20}$$

$$\Pi \approx 2.0 \times 10^{-7}. \tag{21}$$

Since Π is several orders of magnitude smaller than 1, this confirms that gravitational forces are negligible in comparison to contact forces. As a result, pollen motion is dictated by particle interactions, anther vibrations, and boundary collisions, rather than gravitational settling. This validates the assumption that DEM simulations can exclude gravitational effects from Eq. 7 without significantly altering the dynamics of pollen expulsion.

To further illustrate the insignificance of gravitational forces, we estimate the velocity at which gravity and contact forces become comparable ($\Pi = 1$). Setting $\Pi = 1$ in Eq. 15, we solve for v:

$$v = \sqrt{\frac{m_p g}{K_n}}. \tag{22}$$

Substituting known values:

$$v = \sqrt{\frac{(4.2 \times 10^{-10}\ \text{kg})(9.81\ \text{m/s}^2)}{1.6 \times 10^{9}\ \text{N/m}}}. \tag{23}$$

$$v \approx 1.6 \times 10^{-9}\ \text{m/s} = 1.6\ \text{nm/s}. \tag{24}$$

Since this velocity is several orders of magnitude lower than any realistic pollen movement induced by vibrational excitation, gravitational forces remain negligible compared to contact forces. This further confirms that contact interactions are the dominant forces governing pollen expulsion in DEM simulations.

Thus, the final governing equation for pollen motion in DEM simplifies to:

$$m_p \frac{d\mathbf{v}_p}{dt} = \mathbf{F}_c. \tag{25}$$

Implementation in STAR-CCM+

This work splits its discussion based on the type of anther deformation permitted in the simulations. First, a simple translating motion is applied, in which the anther moves as a rigid body without deformation. This approach isolates the role of pollen-pollen interactions and material properties, particularly for simulations incorporating different

restitution coefficients. Second, the anther undergoes deformation following the first two mode shapes of a cantilever beam, allowing for an investigation into how energy transfer from the anther wall influences pollen expulsion dynamics.

The translating simulations, which apply a uniform translation to the entire anther similar to [13], are discussed first. The second set of simulations explores the effects of modal deformation, focusing on how structural vibrations alter pollen expulsion.

DEM in STAR-CCM+

Meshing of "Mesh-free" DEM When applying contact modeling to walls, the term 'mesh-free' DEM can be somewhat misleading, as discretization of the bounding walls is necessary to facilitate particle-wall interactions. In this study, the walls are not static; rather, they move and deform according to prescribed time-dependent equations, which govern their displacement at each moment in the simulation. In a DEM simulation, the walls are represented by a triangulation of the constantly updating surfaces, which serve as surface patches to detect contact. In a simple system where the bounding walls do not deform (or purely translate), this mesh can be relatively coarse, resembling Fig. 3a, where the surface normal is constant everywhere and the intersection of the plane of any triangle is not changed through progressive subdivision. However, if the wall is non-planar and subject to deformation, a finer mesh is required to accurately capture contact points along its surface, as shown in Fig. 3b. In the present simulations, a base mesh size of 1 mm was used to discretize the anther walls with a minimum size of 0.02 mm near the pore, balancing accuracy and computational efficiency. A finer mesh improves contact resolution but increases computational cost, while a coarser mesh may reduce accuracy in tracking deformation and particle-wall interactions.

The importance of finer meshes for deforming walls becomes more evident when considering a side view of the bounding walls. If the wall is initially represented as a

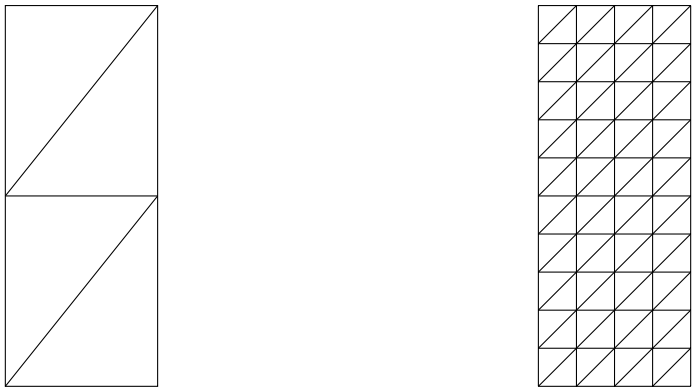

(a) (b)

Figure 3: Comparison of a coarse mesh (left) and a finer mesh (right). (a) Coarse triangular meshing of a wall. (b) Finer triangular meshing with increased resolution.

discretized two-dimensional plane (Fig. 4a), with cells extending into the page, and then deformed into a sinusoidal shape (Fig. 4b), the discrete representation of the mesh (the number, shape, and location of the elements that make up the surface mesh) affects how deformations are captured, as seen in Fig. 5, and therefore how and when particles collide with a wall and in what direction they are accelerated.

To prescribe movement or deformation to the anther walls, time-dependent equations are applied directly to each node of the meshed walls. These equations govern the displacement of each node, ensuring the wall follows a predefined motion throughout the simulation. For simple translation, a uniform equation describing position or velocity over time is applied to all nodes. In contrast, for wall deformations such as sinusoidal oscillations or modal vibrations, the equations must account for individual node positions. This is typically done by expressing displacement as a function of both spatial position (x) and height along the anther (y).

Since deformation is applied only at the mesh nodes, the wall deformation is not truly continuous, as illustrated in Fig. 4b. Instead, the contact points between particles and the wall follow a discretized representation, as shown in Fig. 5. This means that while the prescribed motion defines an idealized smooth deformation, the actual interaction between

Figure 4: Effect of deformation on a discretized bounding wall. (a) Planar wall with evenly spaced nodes. (b) Sinusoidally deformed wall where nodes follow the shape of the deformation.

particles and the wall occurs at discrete mesh points, affecting how forces are transmitted. However, a finer mesh also significantly increases the computational cost of DEM simulations due to the larger number of deformed points requiring calculation and the corresponding increase in particle-wall collision checks.

Figure 5: Comparison of coarse (left) and fine (right) meshing for DEM wall discretization. Finer meshing improves contact accuracy but increases computational cost. The red markers indicate nodal points used for contact detection, with finer meshes capturing more accurate wall deformations.

Time-Stepping In Siemens' SimCenter STAR-CCM+ 2206 [30], the mesh-free DEM model employs an explicit time integration scheme, where selecting an appropriate time step Δt is critical for maintaining numerical stability and ensuring that particle interactions remain physically realistic. For the simulations performed in this study, a fixed time-step of $\Delta t = 5 \cdot 10^{-5}$ seconds was used, ensuring stability while maintaining computational efficiency. If the time step is too large, numerical errors can lead to unrealistic particle overlap or missed collisions, destabilizing the simulation. To prevent these issues, STAR-CCM+ constrains the

time step using the fastest relevant timescale governing particle motion, which is determined by three primary factors: the Rayleigh wave propagation time τ_1 (Eq.26a), the impact duration τ_2 (Eq.26b), and the particle transit time τ_3 (Eq. 26c).

$$\tau_1 = \pi \frac{R}{v_{Rayleigh}}, \tag{26a}$$

$$\tau_2 = 2.94 \left(\frac{5\sqrt{2}\pi\rho}{4} \frac{1-\nu^2}{E} \right)^{\frac{2}{5}} \frac{R}{\sqrt[5]{v_{impact}}}, \tag{26b}$$

$$\tau_3 = \frac{R}{v_{particle}}. \tag{26c}$$

The primary constraint on the DEM time step arises from the assumption that the force acting on a particle is influenced only by its immediate neighbors within a single time-step. This is represented in Eq. 26a, where R is half of the characteristic minimum particle dimension, or in the case of a pollen particle, its radius. The Rayleigh wave velocity $v_{Rayleigh}$ is determined by the material properties of the particle.

The second limiting factor is the duration of an impact between two perfectly elastic particles. For two particles of equal radius R, this is given by Timoshenko (1951) in Eq. 26b where v_{impact} is the impact velocity.

The final constraint, the particle transit time τ_3 (Eq. 26c), prevents particles from passing through other particles or boundary walls. This condition achieves pass-through prevention by ensuring that a particle moves no more than its radius R within ten time steps, where $v_{particle}$ is the particle velocity.

The final time step for an individual particle is determined as the minimum of:

$$\min(\tau_{scale} \cdot \tau_1, \quad 0.1 \cdot \tau_2, \quad 0.1 \cdot \tau_3), \tag{27}$$

where τ_{scale} is a user-defined time-scale within STAR-CCM+. The inclusion of the 0.1 scaling factors for τ_2 and τ_3 provides a stability buffer, ensuring that impact forces and particle motion are resolved with sufficient temporal resolution to prevent numerical artifacts.

Model Definitions

Translating Simulation To simplify the anther geometry and provide a more direct comparison to the existing numerical models, a box approximation was used, which is based on *Solanum lycopersicum* (Solanaceae) as described in [13]. Two geometries were created: a pseudoporicidal anther modeled as an extruded 2D shape similar to [13], resulting in a slit at the apical end, and a poricidal design featuring a finite-sized pore at the apical end to better represent a real pore [7]. Both anther geometries were defined with a width and length of $a = 0.69\,\text{mm}$ and a height of $b = 5.07\,\text{mm}$. Additionally, a hole at the top of the anther was dimensioned as $h = 0.22\,\text{mm}$, such that the pseudoporicidal model's slit accounted for 31.9% of the total top area, while the poricidal model featured a square pore occupying 10.2%. The anther geometries and pore shapes are shown in Fig. 6.

Modeled after the vibration profile described in [13], the anther undergoes strictly translational motion along the y-axis of Fig. 6. The position of the anther wall is given by

$$S_{wall} = \eta(\cos(\omega_1 t) + \cos(\omega_2 t)), \tag{28}$$

and the corresponding velocity is

$$v_{wall} = -\eta(\omega_1 \sin(\omega_1 t) + \omega_2 \sin(\omega_2 t)), \tag{29}$$

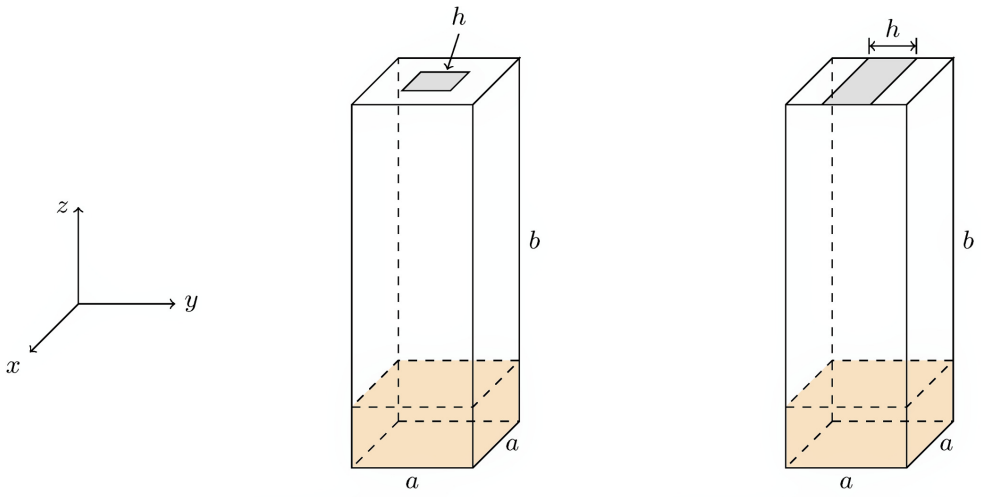

(a) *Poricidal Geometry* **(b)** *Pseudoporicidal Geometry*

Figure 6: Representation of poricidal geometry (right) and pseudoporicidal geometry (left). The orange shaded region indicates where particles are injected, while the gray shaded area represents the pore exit. These geometries approximate anthers found in the *Solanum* family.

where t represents time and η is the half peak displacement amplitude. Due to the two components in S_{wall}, the peak displacement amplitude is 2η and varies from 0.4 mm to 2 mm in increments of 0.4 mm. The frequency ω_1 is varied, while ω_2 remains fixed at 390 Hz. The varied frequencies include 150 Hz, 200 Hz, 300 Hz, and 400 Hz (capturing the biologically relevant buzzing range) and extend from 550 Hz to 1600 Hz in increments of 350 Hz.

This wide frequency range was chosen to allow direct comparison with previous studies [13, 27] and to assess whether modeling provides insight into the influence of frequency on pollen release. Unlike in [13], a fixed ω_2 does not guarantee a beat or pulse at the variable frequency, but it does produce a more organic signal compared to a pure tone. While the chosen excitation frequencies extend beyond the typical 100–400 Hz range observed in bees, artificial pollination technologies are not constrained by biological limitations. Therefore,

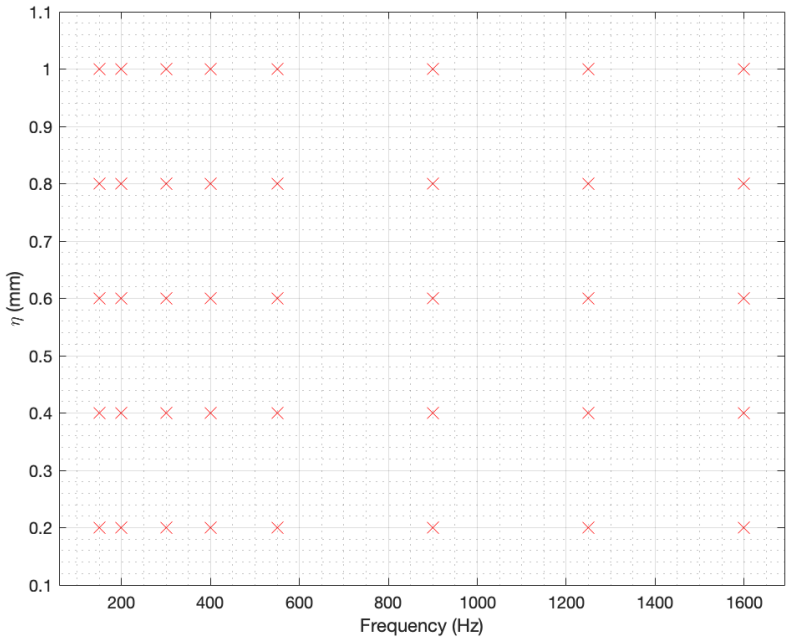

Figure 7: Parameter space of excitation frequencies and displacement amplitudes used in the study. The varied frequencies include biologically relevant buzzing frequencies (150–400 Hz) as well as higher frequencies (550–1600 Hz).

exploring higher frequencies can help determine whether they enhance pollen expulsion.

Each of the 80 simulations involved randomly seeding 10,000 pollen particles in the bottom 5% of the anther, as shown in the shaded region of Fig. 6. The number of pollen grains in an anther varies significantly across plant species. For example, Kemp and Vallejo-Marín reported averages ranging from 22,000 to 466,000 grains for six *Solanum* species [18], while Vallejo-Marín *et al.* observed averages between 29,000 and 800,000 [36]. Harder and Barclay found an average of 1,270,700 grains for *Dodecatheon conjugens* [14].For this work, a comparison between simulations using 10,000 and 100,000 particles showed no significant difference in the results, making the lower count preferable due to reduced computational costs.

The particles were seeded at the bottom of the anther under the assumption that pollen settles in a common area due to agitation, resulting in a packing density of 34.7%.

Lower packing densities would reduce initial particle collisions, slowing pollen release. The coefficients of restitution were set to represent a perfectly elastic system to allow direct comparison with the billiards model for the bulk of the translating simulations, but a subset of simulations were run with varying restitution to determine its significance. Pollen particles were initialized with zero velocity and had properties listed in Table 1.

The Young's modulus of pollen depends on hydration and was approximated based on the work of [25]. Pollen density also varies with hydration [31], with reported values between 968 kg/m^3 and 2238 kg/m^3 [37]. A density of 1000 kg/m^3 was chosen as a representative value. Under perfectly elastic conditions, the Young's modulus acts as a scaling factor for the response time of pollen particles to collisions, while particle mass is ignored. Simulations were run for 0.5 s with a time step of $\Delta t = 1\,\mu s$.

Table 1: Pollen properties [4]* [23]† [25]‡ and simulation values§.

Variable	Value
$E^{\ddagger}$	1.6 GPa
ν^{*}	0.45
$\rho^{\S}$	1000 kg/m^3
$R^{\dagger}$	0.01 mm
${C_{n\ rest}}^{\S}$	1.0
${C_{t\ rest}}^{\S}$	1.0
${v_0}^{\S}$	0 m/s

Modally Deforming Simulations In addition to the strictly translational simulations, a set of modal vibration simulations was performed to investigate the effect of the shape of anther deformation on pollen expulsion. These simulations used the same pollen and wall material properties as before (assuming a coefficient of restitution equal to 1), but the anther geometry was modified, and a deformation profile was prescribed.

The new anther geometry was cylindrical, with a height of $h = 8.9$ mm, a radius of $r = 0.28$ mm, and a hole diameter of $r_h = 0.089$ mm. These values were selected to align more closely with ongoing experimental studies and differ from the translating anther geometries,

which had a box-like structure with a height of $b = 5.07$ mm and a square cross-section of width $a = 0.69$ mm.

The cylindrical shape introduces key differences from the box-like geometries used in the translating simulations. First, the curved inner surface further alters the direction of particle reflections upon impact, potentially influencing the distribution and trajectory of pollen grains. Unlike planar walls that reflect particles in predictable directions, the curvature of the cylindrical anther can create a more varied dispersion of pollen grains inside the anther, potentially affecting expulsion efficiency.

Second, the cylindrical geometry results in a smaller surface area experiencing the highest velocities during vibration. In contrast to a flat wall that moves uniformly, the deformation profile of a cylindrical anther creates spatial variations in velocity amplitude, which could affect how efficiently energy is transferred to pollen grains. Additionally, the modal deformations propagate differently through the anther structure, potentially leading to variations in pollen expulsion dynamics compared to the translating cases.

The dimensions of the cylindrical anther also introduce additional differences in how pollen is moved within the anther. The overall height is greater than that of the translating anther, which may allow for more sustained pollen-pollen interactions before grains reach the pore. The smaller pore size ($r_h = 0.089$ mm) relative to the square poricidal opening of the translating anther ($h = 0.22$ mm) could also influence the rate at which pollen exits the structure. Future comparisons between these models will help assess the relative impact of geometry, deformation mode, and vibration parameters on pollen release.

The displacement of the anther walls in the x-direction along its height is described by Eqs. 30 and 31, where ϕ_1 and ϕ_2 are the modal deformations, η is the peak tip displacement:

$$S_{wall_1} = \eta \sin(\omega t) \cdot \phi_1, \tag{30}$$

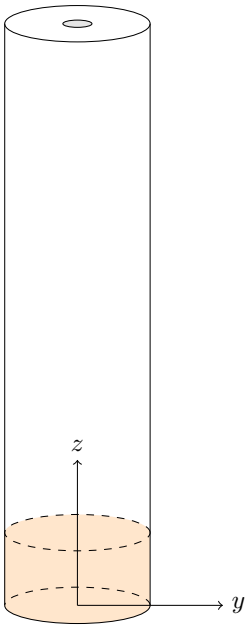

Figure 8: Representation of the poricidal deforming geometry. The orange shaded volume represents the region where particles are injected, while the gray shaded area represents the pore exit.

$$S_{wall_2} = \eta \sin(\omega t) \cdot \phi_2. \tag{31}$$

The mode shapes ϕ_1 and ϕ_2 are given by Eqs. 32 and 33, where k_1 and k_2 are wave numbers determined by the anther geometry, and z represents the height along the anther's length:

$$\phi_1 = \frac{1}{2}\left(\cos(k_1 \cdot z) - \cosh(k_1 \cdot z) + C \cdot (\sin(k_1 \cdot z) - \sinh(k_1 \cdot z))\right), \tag{32}$$

$$\phi_2 = \frac{1}{2}\left(\cos(k_2 \cdot z) - \cosh(k_2 \cdot z) + C \cdot (\sin(k_2 \cdot z) - \sinh(k_2 \cdot z))\right). \tag{33}$$

The resulting deformation profiles are shown in Fig. 9.

To investigate the effects of vibration frequency and displacement amplitude on pollen expulsion, eight parameter sets were evaluated. The two tested frequencies (100 Hz and 400 Hz) were selected to represent the range of biologically relevant vibrations observed in buzz pollination. Two displacement amplitudes 1×10^{-3} m and 1×10^{-4} m were chosen to encompass expected variations in anther deformation, yielding for four simulations for both mode 1 and mode 2 deformations.

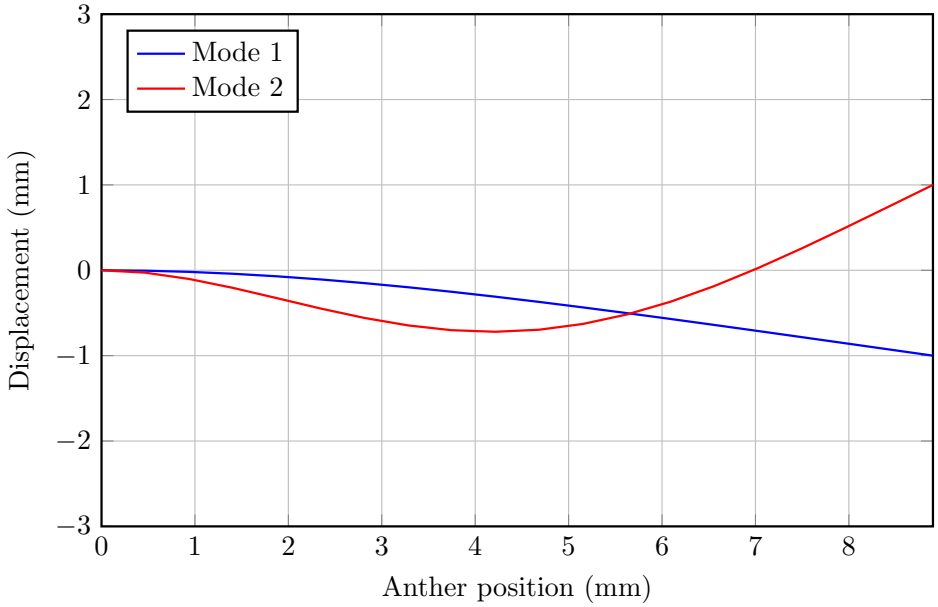

Figure 9: Comparison of the first and second mode shapes of the vibrating anther structure. The displacements are normalized such that the maximum tip displacement is 1 mm. The x-axis represents the position along the anther, while the y-axis shows the corresponding displacement magnitude for each mode.

RESULTS

This chapter presents the results of the discrete element method (DEM) simulations, focusing on the expulsion of pollen from vibrating anthers. The results are divided into two primary sections: translating anther simulations and deforming anther simulations. Each section explores different aspects of pollen expulsion, including the role of pollen-pollen interactions, overall expulsion trends, and expulsion rates across parameter sets.

Translating Anther Simulations

Pollen Expulsion Trends Over Time

In introducing a new numerical model to investigate buzz pollination, part of the initial intent of this study was to compare results from DEM to those observed in Hansen [13] after 1.0 second across the entire parameter space. However, as shown in Fig. 10, by 0.5 seconds, every simulation had already reached full expulsion. This lack of variation provided no meaningful insight into how vibration parameters influenced pollen expulsion. To determine whether displacement amplitude and frequency played a role at earlier stages of the simulations, we examined pollen expulsion trends at earlier times.

We then turned to pollen release at 0.05 s (Fig. 11). Unlike the previous plot, this figure revealed a clear trend: simulations with higher displacement amplitudes and frequencies exhibited significantly greater pollen expulsion at this early stage. This provided the first strong evidence that frequency and amplitude meaningfully influence expulsion rates, even if total expulsion is eventually achieved across all conditions.

Examining pollen expulsion at earlier times revealed how vibration parameters influence expulsion rates in greater detail. While total expulsion was nearly universal by 0.5 s, the earlier time steps clearly demonstrated that pollen release rates are strongly dependent on displacement amplitude and frequency.

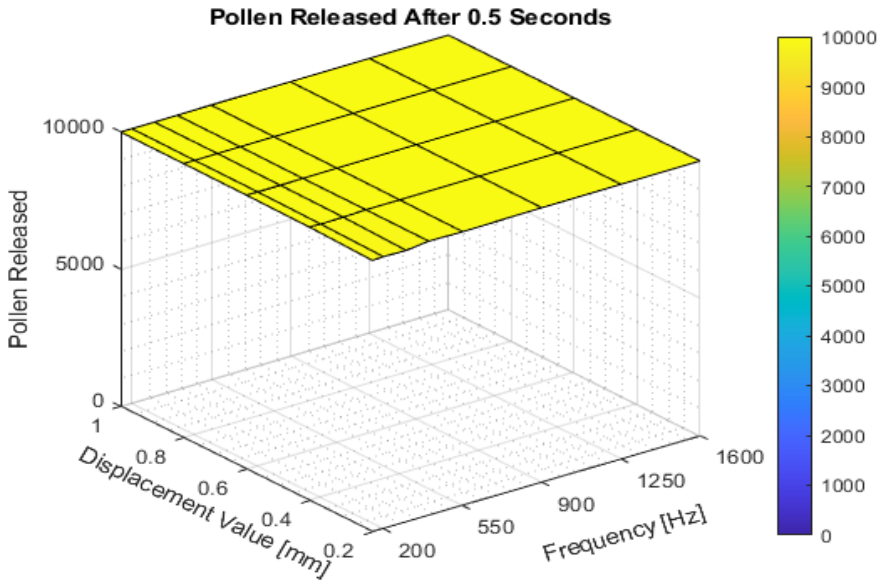

Figure 10: Total pollen released after 0.5 seconds as a function of displacement amplitude and frequency. Some variation is observed, but most simulations still approach full expulsion, suggesting that key differences occur earlier in the process.

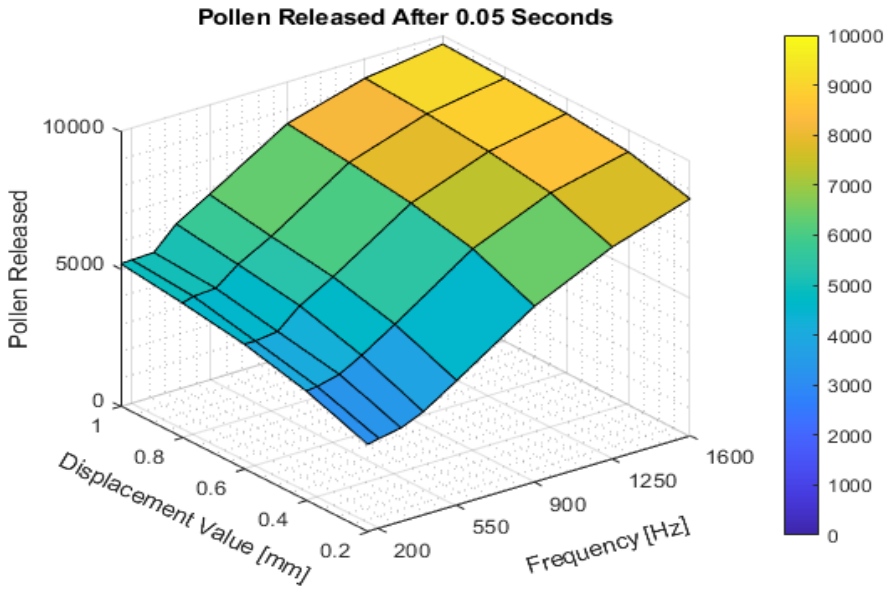

Figure 11: Total pollen released after 0.05 seconds as a function of displacement amplitude and frequency. At this early time step, a strong trend emerges, showing that higher frequencies and displacement values correspond to faster pollen expulsion. This pattern closely aligns with trends observed in Hansen et al. [13].

By examining total pollen expulsion at $t = 0.05$ s, we observed that higher frequencies and displacement amplitudes led to significantly faster expulsion. This indicated that while all tested excitation conditions ultimately achieved full pollen release, their rate of expulsion varied substantially depending on the vibration parameters.

These findings align with prior work on vibrational pollen release, particularly the frequency-dependent expulsion trends identified by Hansen et al. [13] and the acceleration-driven expulsion dynamics reported by Rosi-Denadai et al. [27]. Our DEM simulations exhibited faster expulsion timescales compared to these experimental measurements but captured the same overall dependence on vibration frequency and displacement amplitude. This agreement provides an independent confirmation of the key vibrational parameters governing pollen release and offers a more systematic framework for quantifying expulsion dynamics across a range of conditions.

Pollen-Pollen vs. Pollen-Wall Interactions Over Time

To assess the significance of pollen-pollen interactions in the translating anther simulations, the average number of pollen-pollen and pollen-wall collisions was tracked over time across all simulations. These interactions were analyzed separately for both the poricidal and pseudoporicidal geometries which provides an early idea of how the pore size influences these results. Figure 12 reveals distinct differences in pollen-pollen vs. pollen-wall interactions across the two geometries. In both cases, pollen-pollen collisions initially increase but plateau as particles disperse. However, pollen-wall interactions dominate for the poricidal geometry likely because the smaller exit restricts how quickly pollen is expelled forcing more wall interactions, but with increasingly large distances between pollen particles as their numbers decrease over time.

The pseudoporicidal geometry exhibits a higher relative proportion of pollen-pollen interactions throughout the simulation. This is most likely due to the lower surface area

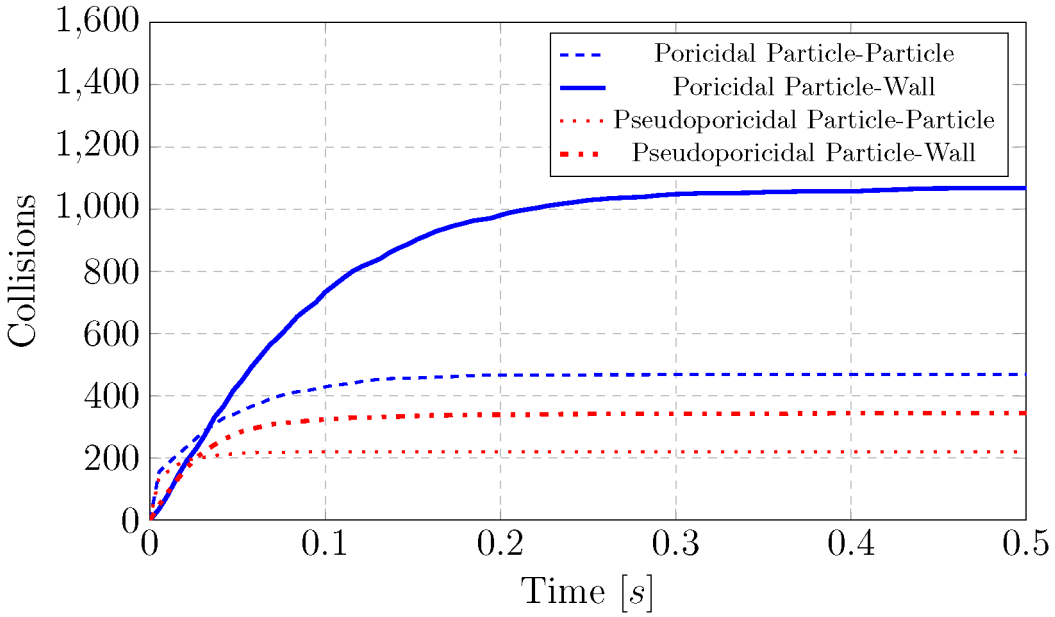

Figure 12: Average number of pollen-pollen and pollen-wall interactions over time for poricidal and pseudoporicidal geometries. The poricidal geometry (blue) exhibits a higher overall number of collisions, particularly for pollen-wall interactions, whereas the pseudoporicidal geometry (red) has a lower amount of collisions.

standing in the way of pollen expulsion.

The translating anther simulations provided a controlled environment to isolate and examine the granular dynamics governing pollen expulsion. A key finding was the critical role of pollen-pollen interactions. Unlike models that assume pollen grains behave as independent particles, these simulations demonstrated that inter-particle collisions are a dominant mechanism in guiding grains toward the anther pore. The significance of this effect was present in both poricidal and pseudoporicidal geometries but inter-particle interactions were more pronounced in the latter due to the wider ejection area. By explicitly modeling these interactions, we were able to eliminate the need for predefining an initial pollen velocity, as the cumulative effect of particle collisions and energy transfer naturally drove pollen movement. This approach captures a more physically representative mechanism of pollen transport, where the anther's vibrations induce inter-particle interactions that ultimately

dictate expulsion rather than relying on predefined motion.

Examining the temporal evolution of these interactions revealed two distinct phases in the expulsion process. In the early stages of vibration, pollen grains experience frequent collisions with one another, leading to a rapid redistribution of trajectories. This high initial rate of inter-particle interactions allows for an efficient spread of kinetic energy throughout the pollen cluster, generating a broad distribution of particle velocities and directions. As the simulation progresses and pollen grains begin to separate, the dominance of inter-particle interactions diminishes, and particle-wall collisions become the primary mechanism governing expulsion. This shift in interaction dynamics highlights the transition from a highly coupled granular system to a more ballistic regime, where individual pollen grains predominantly interact with the vibrating anther walls before eventual ejection.

This study contrasts with previous work by Hansen et al. [13], where pollen grains were assigned an initial velocity rather than gaining momentum through repeated collisions. While this assumption provided a simplified means of modeling expulsion, our findings suggest that inter-particle energy transfer plays a fundamental role in determining pollen trajectories, reinforcing the necessity of treating pollen expulsion as a granular process rather than a system of independent particles. Particle-particle collisions accounted for an average across the parameter sweep of $30.03 \pm 1.32\%$ and $39.50 \pm 2.67\%$ of all collisions in poricidal and pseudoporicidal anthers, respectively.

Comparing poricidal and pseudoporicidal geometries further illustrates the effect of boundary constraints on pollen interactions. In the poricidal case, pollen grains encounter more wall collisions before exiting, leading to a greater overall number of particle-wall interactions. In contrast, the pseudoporicidal anther allows for a wider dispersal of pollen grains upon release, reducing the relative fraction of wall interactions compared to inter-particle collisions. However, in both and cases across the range of parameters tested, the transition from early-stage inter-particle interactions to late-stage wall interactions remains

consistent, reinforcing the conclusion that particle collisions serve as an intermediate step in the pollen expulsion process before anther vibrations ultimately drive expulsion.

Quantifying Pollen Expulsion Rates

To understand how different vibration parameters influence pollen expulsion, we first examine how the number of expelled pollen grains evolves over time. Observing this time-dependent expulsion behavior is critical for identifying trends that may not be apparent when analyzing only the total expelled pollen at a single time step.

Figure 13 presents representative examples of pollen expulsion over time for both poricidal and pseudoporicidal anther geometries. The curves reveal an initial period of rapid expulsion, followed by a gradual slowdown as fewer grains remain available for ejection. As seen in Fig. 13, the expulsion curves exhibit an approximately linear region during the early-to-mid expulsion phase, a trend consistently observed across all translating anther models. To characterize expulsion rates across simulations, we define a characteristic time, $t_{1/2}$, as the time at which 50% of the initial pollen grains have been expelled. While other points such as $t_{1/4}$ or $t_{2/3}$ could similarly be used, $t_{1/2}$ provides a convenient and robust reference point near the center of the linear expulsion period. It should be noted that $t_{1/2}$ does not necessarily mark the end of linear expulsion behavior, but rather serves as a consistent measurement point across cases.

To characterize the rate of pollen expulsion, we define $\dot{P}$ as the slope of the expulsion curve evaluated at $t_{1/2}$, the time at which half of the initial pollen grains have been expelled. This provides a consistent measure of the active expulsion phase across simulations, avoiding the brief initial delay before particle expulsion begins and excluding late-time plateauing once most pollen has been expelled.

While the expulsion rate $\dot{P}$ provides a consistent metric for comparing different simulations, it does not directly explain why certain vibration parameters result in faster or

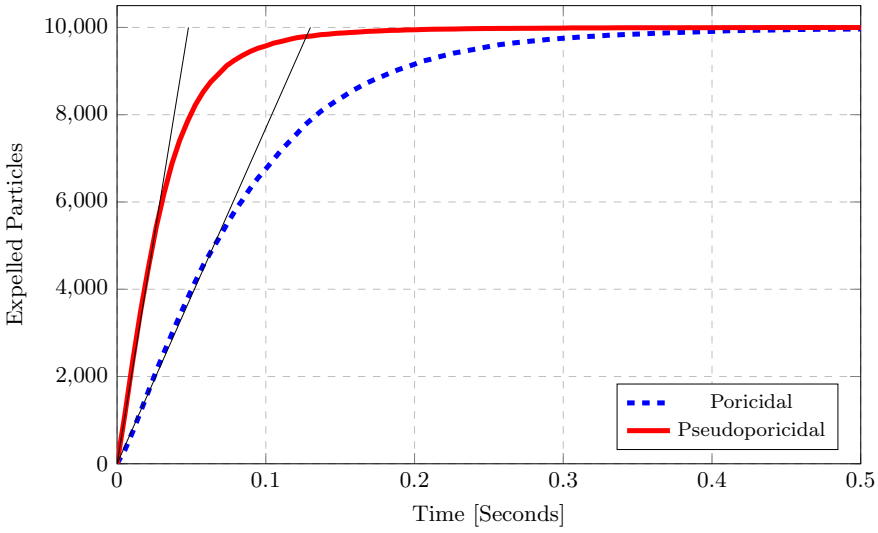

Figure 13: Examples of pollen expulsion over time for poricidal and pseudoporicidal geometries at $\eta = 0.4$ mm and $\omega_1 = 150$ Hz, seeded with 10,000 particles. The thin lines illustrate early expulsion trends; formal expulsion rates, $\dot{P}$, are evaluated at $t_{1/2}$.

slower pollen release. Prior studies have proposed that peak velocity or acceleration may influence pollen expulsion [7, 13, 27]. However, these quantities alone do not fully account for the observed variation in expulsion rates across different excitation conditions. Motivated by this, we explored whether jerk—the time derivative of acceleration—could serve as a stronger unifying parameter.

Jerk (J) is defined as the time derivative of acceleration, which can be obtained by differentiating position with respect to time. Starting from the displacement of the anther:

1. **Position** ($x(t)$):

$$x(t) = \eta \cos(\omega t), \tag{34}$$

where η is the displacement amplitude and ω is the angular frequency of vibration.

2. **Velocity** ($V(t)$) is the first derivative of position:

$$V(t) = \frac{dx}{dt} = -\eta\omega \sin(\omega t). \tag{35}$$

3. **Acceleration** ($A(t)$) is the first derivative of velocity:

$$A(t) = \frac{dV}{dt} = -\eta\omega^2 \cos(\omega t). \tag{36}$$

4. **Jerk** ($J(t)$) is the first derivative of acceleration:

$$J(t) = \frac{dA}{dt} = \eta\omega^3 \sin(\omega t). \tag{37}$$

To simplify the time dependence and focus on the maximum vibrational forcing, we consider the peak value of jerk, which occurs when $\sin(\omega t) = 1$, yielding:

$$J_{\max} = \eta\omega^3. \tag{38}$$

To evaluate the relationship between vibrational parameters and pollen expulsion, we compared the expulsion rate $\dot{P}$ against three quantities: maximum velocity ($V_{\max}$), maximum acceleration ($A_{\max}$), and maximum jerk ($J_{\max}$). Figure 14 presents these comparisons across the full set of simulations.

The results indicate that while both velocity and acceleration relate to pollen expulsion rates to some extent, jerk provides a stronger correlation across different excitation conditions. This trend suggests that the rate of change of acceleration may play a key role in pollen release dynamics.

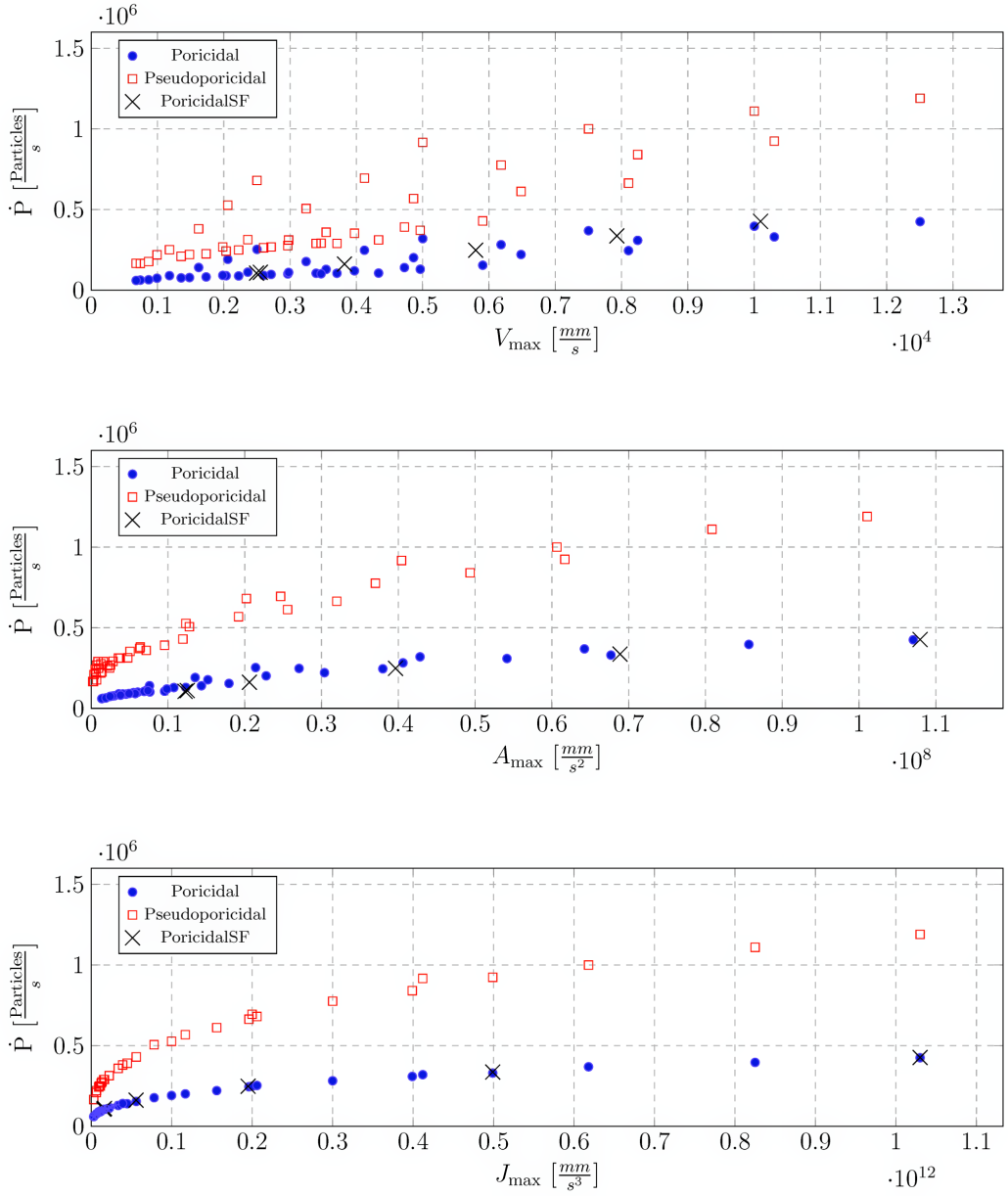

Figure 14: Comparison of pollen expulsion rate ($\dot{P}$) as a function of maximum velocity ($V_{\max}$), maximum acceleration ($A_{\max}$), and maximum jerk ($J_{\max}$). While velocity and acceleration show some correlation with expulsion rates, the strongest collapse of data is observed when plotted against jerk.

These findings suggest that jerk may serve as a unifying descriptor of pollen expulsion dynamics across different vibration conditions. This approach simplifies the analysis of expulsion behavior and offers insight into the dynamic forces governing pollen release.

While prior studies examined displacement, velocity, and acceleration as factors influencing pollen expulsion [7, 13, 27], these parameters do not fully capture variations across different excitation conditions. This study systematically analyzes the role of jerk ($J_{\max} = \eta\omega^3$) and finds that it exhibits a stronger correlation with expulsion rate than either velocity or acceleration, offering a more comprehensive framework for understanding pollen release dynamics.

These observations imply that the rate of change of acceleration, rather than peak acceleration alone, plays a critical role in pollen expulsion. Unlike velocity and acceleration, which describe the magnitude of motion, jerk characterizes how quickly forces within the anther fluctuate, offering a more direct connection to the dynamic energy transfer necessary for efficient pollen ejection. The strong correlation between jerk and expulsion rate suggests that frequency influences pollen release not only by determining peak forces but also by modulating the rate at which forces vary during vibration.

Potential applications of this framework could extend to artificial pollination technologies. Optimizing vibratory excitation profiles to target specific jerk values may offer a way to enhance pollen release efficiency in agricultural systems, particularly for crops that rely on vibratory pollen extraction. Future studies could explore the use of jerk as a predictive tool for selecting appropriate combinations of excitation frequency and displacement amplitude to achieve desired expulsion characteristics.

Effects of Restitution Coefficient on Pollen Expulsion

To investigate the role of energy dissipation in pollen expulsion, simulations were performed using different normal restitution coefficients (C_{rest}) of 0.25, 0.5, 0.75, and 1.0.

These values represent varying degrees of inelasticity, where lower restitution coefficients correspond to greater energy loss during collisions. The same restitution coefficient was applied uniformly to both pollen-pollen and pollen-wall interactions. The restitution sweep simulations were conducted at a fixed displacement amplitude of $\eta = 0.6$ mm and an excitation frequency of $\omega = 550$ Hz, using a poricidal anther seeded with 10,000 particles. This analysis aimed to assess how varying levels of energy dissipation influence particle motion and subsequent pollen expulsion rates.

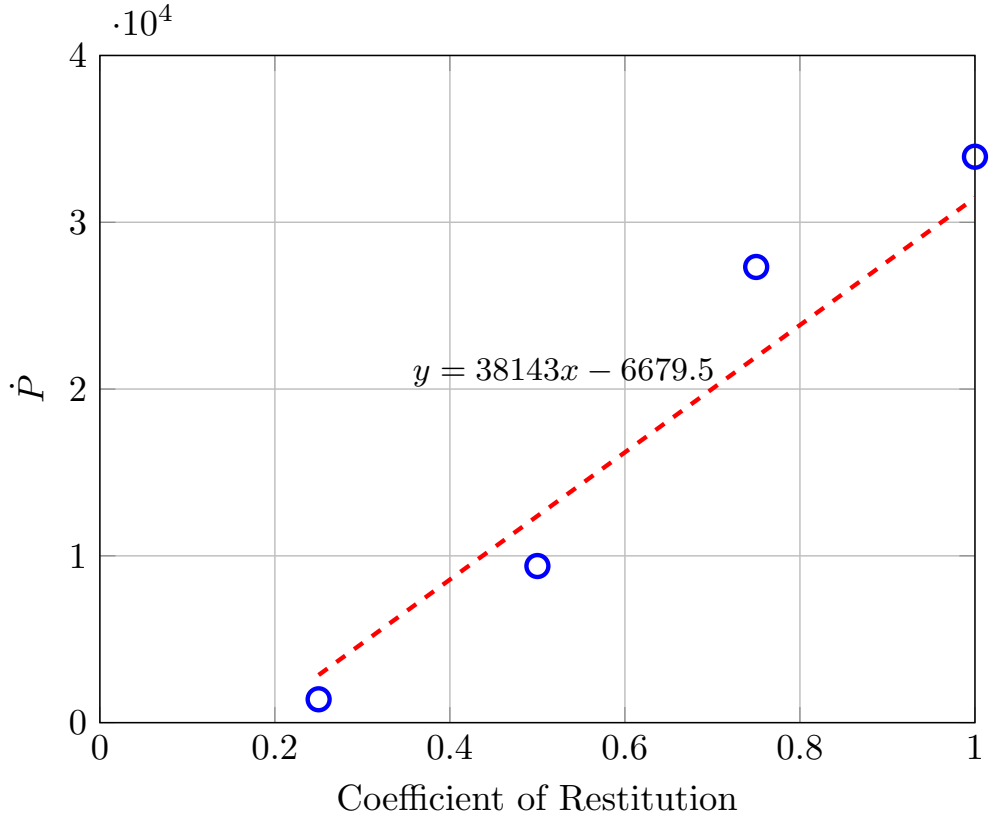

Figure 15: Relationship between restitution coefficient and pollen expulsion rate. As restitution increases, the rate of pollen expulsion rises approximately linearly, indicating that more elastic collisions enhance particle mobility and expulsion efficiency.

Figure 15 shows how pollen expulsion rate scales with the restitution coefficient. The data reveal an approximately linear relationship: as restitution increases, so does the expulsion rate. This suggests that more elastic collisions allow particles to retain kinetic

energy longer, increasing their likelihood of reaching the pore and escaping.

At lower restitution values (e.g., $C_{\text{rest}} = 0.25$), collisions are highly dissipative—particles lose a greater fraction of their kinetic energy during each impact, making it more difficult for grains to sustain the momentum needed for expulsion. In contrast, at $C_{\text{rest}} = 1.0$, collisions are fully elastic, allowing particles to retain kinetic energy across successive interactions and contributing to higher cumulative expulsion rates.

This trend suggests that while the general mechanism remains consistent, restitution modulates the intensity of expulsion, effectively acting as a multiplier on particle escape rates.

Deforming Anther Simulations

The deforming anther simulations introduce an additional layer of complexity by altering the spatial distribution of collision forces along the anther walls, in contrast to the purely translating cases. Rather than conducting an exhaustive parameter sweep, these simulations focused on targeted investigations of how structural vibration modes—specifically, the first and second natural modes of a cantilever beam—affect total pollen expulsion, expulsion rates, and the roles of inter-particle and particle-wall interactions.

Overview of Modal Deformations

Due to the increased computational complexity of modeling anther deformation that arises from an increased amount of time spent computing wall interactions, a limited number of parameter sets were examined. Both mode shape displacements tested at four different parameter sets, allowing for direct comparisons of how deformation patterns affect the timing and extent of pollen expulsion.

Mode 1 exhibits a deformation pattern that produces a displacement that increases along its length from the base to its pore, potentially leading to steady and direct pollen

ejection. Mode 2 follows a more spatially complex deformation where displacement varies along the anther in both amplitude and direction, potentially influencing pollen trajectories before expulsion. The mode shapes were seen in Fig. 9.

Total Pollen Expulsion Over Time

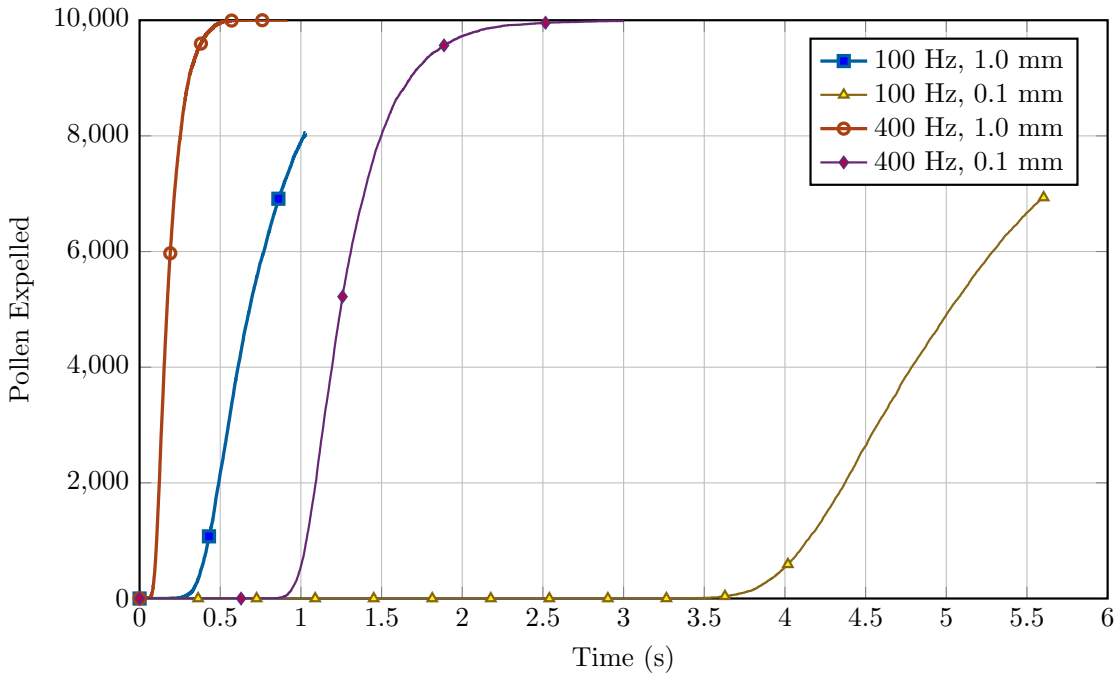

Figure 16: Cumulative pollen expulsion over time for Mode 1 deformation across all tested parameter sets. Each line represents the number of expelled particles over time for a different combination of vibration parameters.

Figures 16 and 17 show cumulative pollen expulsion over time for each mode across all tested parameter sets. These results illustrate how deformation pattern influences the timing of particle expulsion. Although not all simulations ran to full completion due to computational constraints, they progressed far enough to reveal key trends in mobilization behavior.

Across both mode shapes, high-frequency conditions led to faster total expulsion than low-frequency vibrations. This outcome is consistent with the scaling of jerk, where a fourfold increase in frequency results in a 64-fold increase in $J_{\max}$, while a tenfold increase

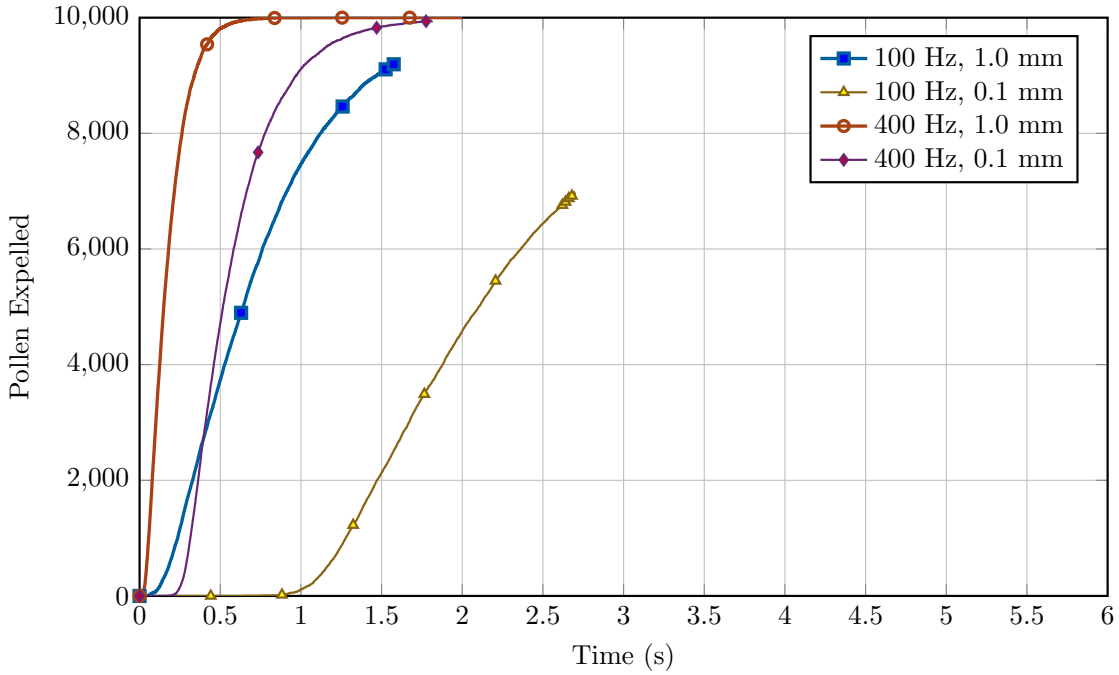

Figure 17: Cumulative pollen expulsion over time for Mode 2 deformation across all tested parameter sets. Each line shows the number of expelled particles over time for a different parameter set.

in displacement produces only a tenfold change in $J_{\max}$. In both mode shapes, simulations with 400 Hz excitation and 1 mm displacement exhibited rapid expulsion within the first second, often reaching high levels of release before the other cases progressed significantly.

For Mode 1 deformations, pollen expulsion curves were distinct and well-stratified across all tested vibration conditions. Higher frequency and amplitude combinations produced faster expulsion, while lower-energy cases expelled pollen more slowly, with minimal overlap between curves. In contrast, Mode 2 simulations exhibited a much more rapid onset of pollen expulsion across all conditions. However, expulsion profiles for different excitation parameters overlapped considerably, particularly at intermediate times. This behavior likely reflects the spatial deformation characteristics of Mode 2, which involve larger displacements near the base of the anther. In the seeded region of the anthers, displacement in Mode 2 was approximately 5.9 times greater than in Mode 1, likely contributing to the more rapid

initial mobilization observed in Mode 2 cases.

Pollen-Pollen and Pollen-Wall Interactions in Deforming Anthers

To further characterize pollen motion during modal deformation, the relative number of particle-particle and particle-wall interactions were tracked over time. These interactions provide insight into how momentum is redistributed among grains and how vibrational energy from the anther walls drives expulsion.

Figures 18 and 19 present the cumulative evolution of these interactions for Mode 1 and Mode 2 deformations across all tested parameter sets.

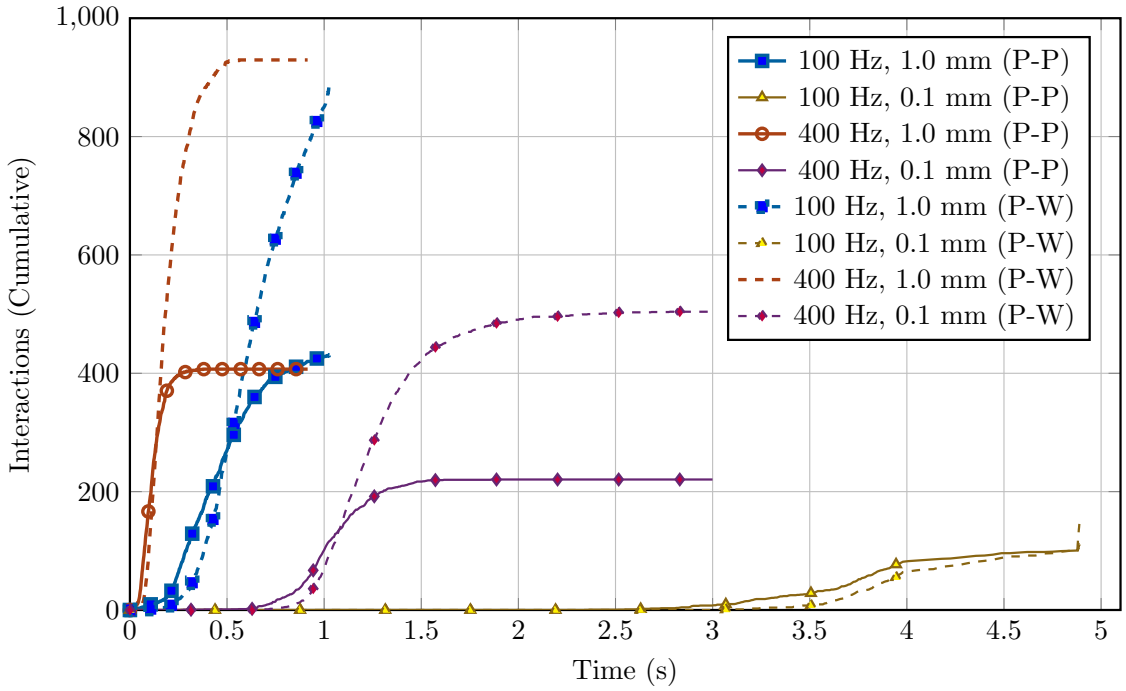

Figure 18: Cumulative particle-particle and particle-wall interactions over time for Mode 1 deformation across all tested parameter sets. Solid lines represent particle-particle interactions, and dotted lines represent particle-wall interactions.

The overall trends remain broadly consistent with those observed in translating anther simulations. Particle-particle interactions dominate early in the simulation, redistributing energy among grains, while particle-wall interactions steadily accumulate and ultimately

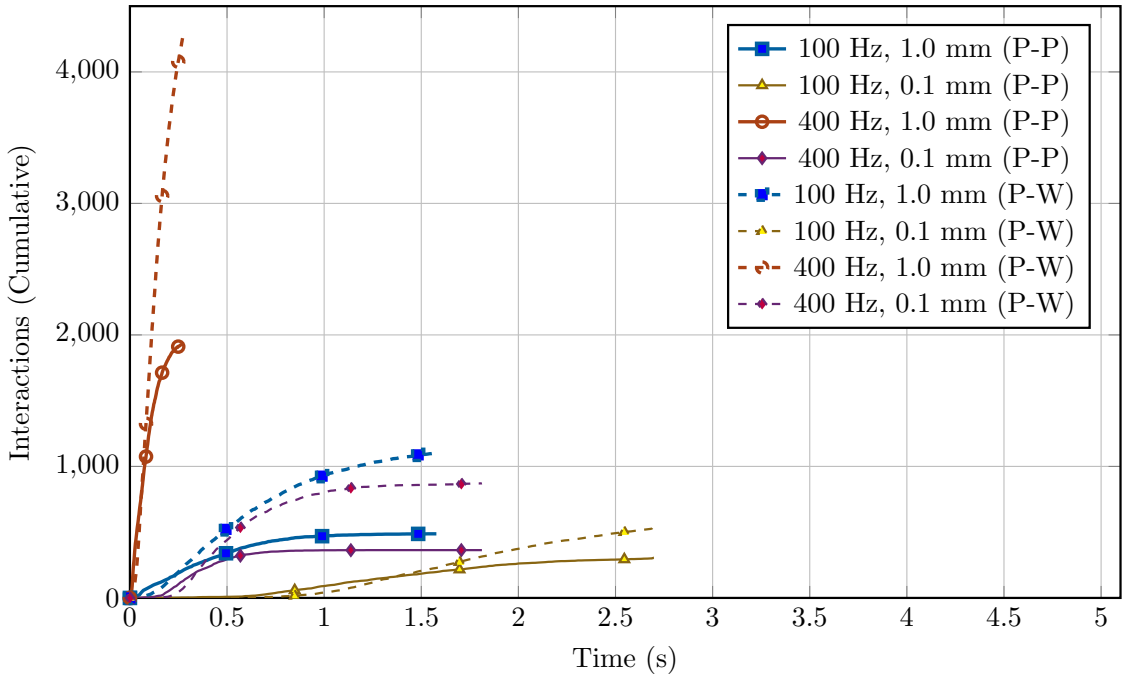

Figure 19: Cumulative particle-particle and particle-wall interactions over time for Mode 2 deformation across all tested parameter sets. Solid lines represent particle-particle interactions, and dotted lines represent particle-wall interactions.

drive expulsion.

In deforming anther simulations, both types of interactions increased steadily over time, with particle-wall collisions accumulating at slightly higher rates across both mode shapes. This indicates that, despite the added complexity of modal deformation, the fundamental dynamics governing pollen expulsion remain consistent: energy transfer from the walls and momentum exchange among grains jointly shape particle trajectories and release behavior.

Timing and Speed of Pollen Expulsion in Deforming Anthers

To further explore the temporal dynamics of modal pollen expulsion, two metrics are introduced to quantify both the initiation and rate of particle release relative to the startup delay of expulsion. The first metric, *start time*, was defined as the time at which the first particle was expelled. The second metric, $\dot{P}$, measured the average particle loss rate between 9000 and 5000 particles. This window was chosen to capture the sustained phase of pollen

expulsion, excluding transient and plateauing behavior.

Figure 20 and Figure 21 visualize these metrics across all tested parameter sets and both deformation modes. The x-axes of the bar charts are intentionally ordered differently to emphasize a key observation: the factors influencing the timing of expulsion do not necessarily align with those affecting the expulsion rate.

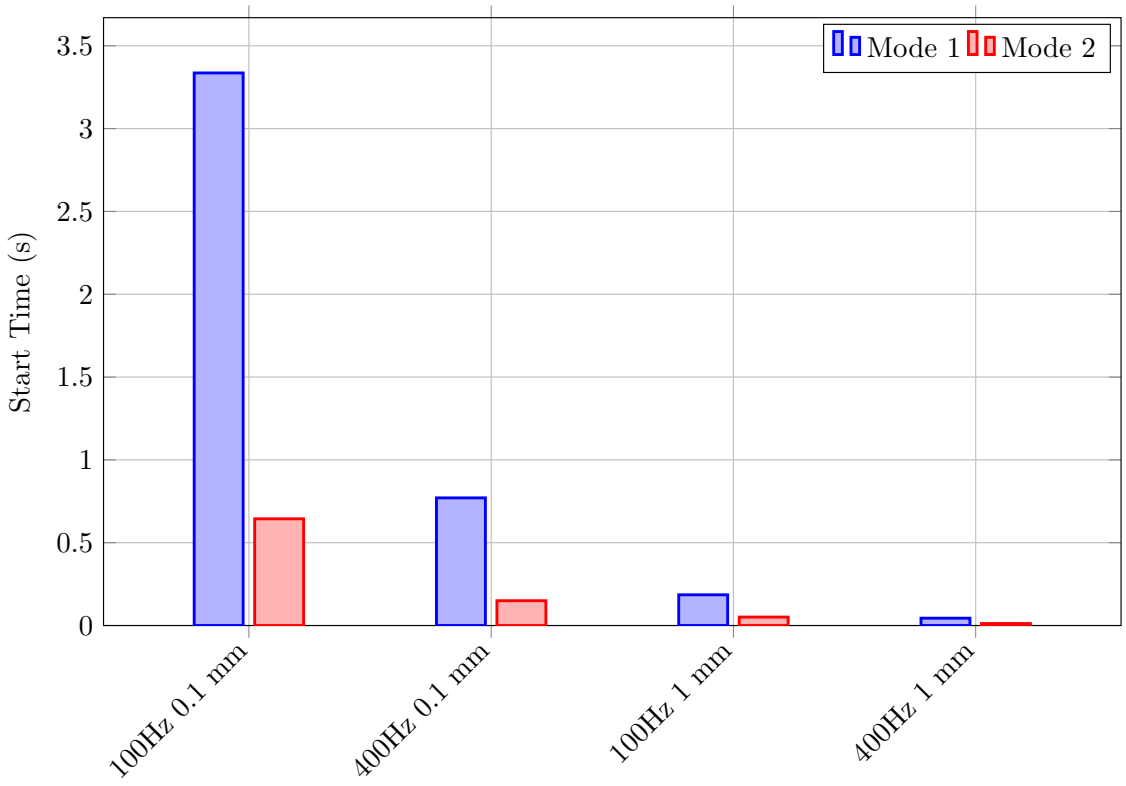

Figure 20: Grouped bar chart showing the start time of pollen expulsion for Mode 1 and Mode 2 across all tested parameter sets. Start time is defined as the moment the particle count first drops below the initial seed count, marking the onset of measurable pollen motion. Comparisons across modes reveal differences in how quickly expulsion is initiated under different deformation conditions.

These results provide an initial perspective on how deformation mode influences both the timing and speed of pollen expulsion. As shown in Fig. 20, Mode 2 consistently initiates particle motion earlier across all parameter sets. This trend is particularly evident at lower amplitude cases such as 100 Hz, 0.1 mm, where Mode 1 exhibits significantly delayed onset

compared to Mode 2. The spatially complex deformation of Mode 2 appears more effective at triggering early particle mobilization.

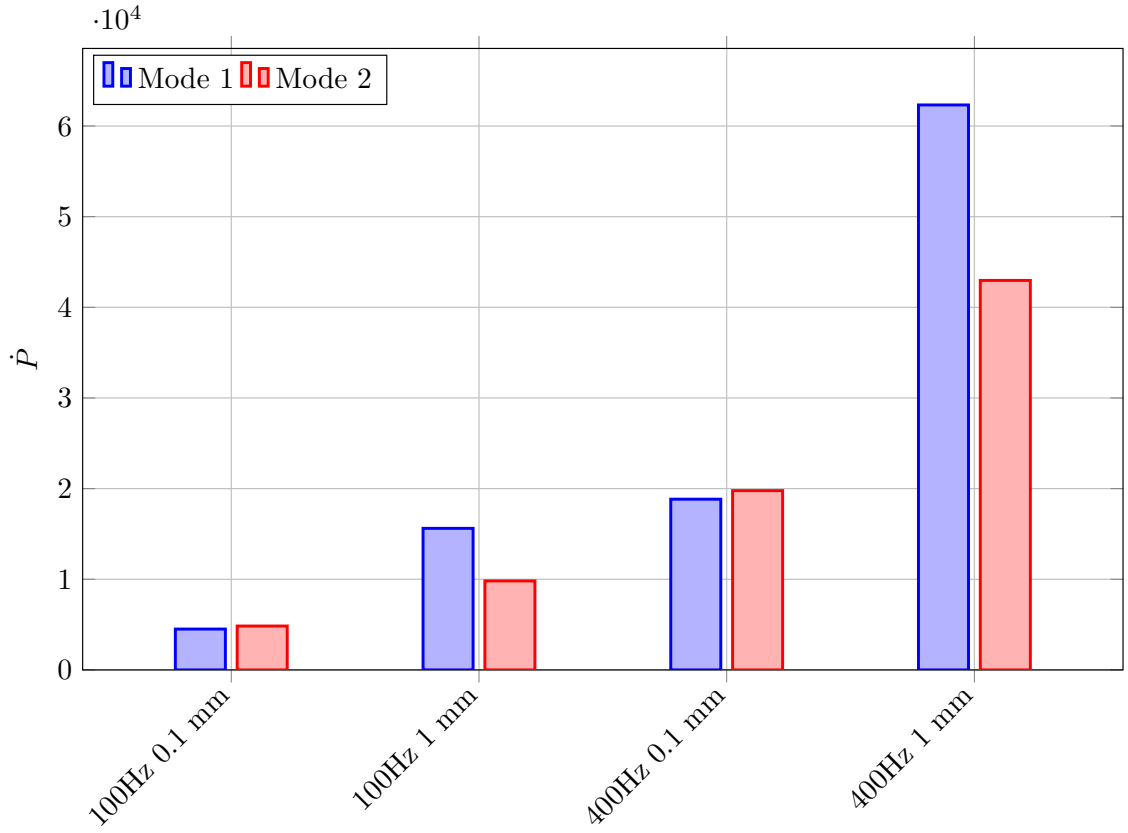

Figure 21: Grouped bar chart comparing the active pollen expulsion rate between Mode 1 and Mode 2 across all parameter sets. Active expulsion rate is calculated as the average rate of particle loss between 9000 particles and 5000 particles. These values represent the sustained release phase after the onset of expulsion, capturing how each mode facilitates particle ejection.

However, as illustrated in Fig. 21, Mode 1 often achieves higher active expulsion rates, especially under high-energy conditions like 400 Hz, 1.0 mm. This suggests that once particle motion is initiated, the more uniform and sweeping deformation of Mode 1 is better suited to sustaining momentum and continuously directing pollen toward the pore. Together, these findings show that the mode shape not only influences whether pollen is expelled, but also when and how efficiently it happens.

Comparison with Translating Anther Dynamics

Comparing deforming anther simulations to translating anther results reveals important differences and similarities in pollen expulsion mechanisms. Although the general roles of particle-particle and particle-wall interactions remained consistent, the introduction of modal deformation highlighted how spatial complexity in deformation patterns can distinctly influence the timing and rate of pollen expulsion.

Unlike translating simulations, where vibration parameters such as frequency and displacement amplitude primarily determined expulsion characteristics, modal deformation introduced additional spatially dependent factors influencing both initiation and active expulsion phases. The contrasting temporal dynamics observed between Mode 1 and Mode 2 demonstrate how different vibrational modes can uniquely modulate pollen expulsion strategies beyond what was observed under purely translating conditions.

In translating anther simulations, jerk emerged as a robust governing parameter, effectively capturing combined effects of frequency and displacement amplitude on expulsion dynamics. However, in deforming anther simulations the distribution of jerk and the location of maximum jerk along the anther are constantly changing, possibly requiring a modified version to make one-to-one comparisons. Future investigations could focus on identifying or developing parameters that effectively incorporate spatial variability in deformation, thus providing a more comprehensive framework for predicting pollen expulsion under realistic, structurally complex vibration scenarios.

CONCLUSION

The Research Goal

The goal of this research was to investigate the dynamics of pollen expulsion in buzz-pollinated anthers using the Discrete Element Method. Buzz pollination is a biomechanical process in which pollinators, primarily bees, apply vibrational forces to anthers to release pollen through specialized pores. While prior experimental studies have examined the frequencies and amplitudes associated with effective pollen ejection, the underlying granular mechanics of pollen motion remain poorly understood.

This study sought to address these gaps by developing a computational model capable of simulating pollen expulsion under vibratory excitation. Two primary simulation approaches were employed:

1. **Translating Anther Simulations** – These simulations eliminated anther deformation, focusing solely on pollen motion under sinusoidal excitation. This approach allowed for an in-depth examination of pollen-pollen interactions, expulsion rates, and the role of vibration parameters in determining ejection dynamics.

2. **Deforming Anther Simulations** – These simulations introduced modal anther deformations, modeled after the first and second vibrational modes of a cantilever beam. The goal was to assess how deformation patterns influence the transfer of energy from the anther walls to the pollen, thereby affecting expulsion.

By systematically varying excitation frequency, displacement amplitude, and anther deformation mode, this study aimed to quantify the factors that most significantly influence pollen expulsion. The results provide new insight into the mechanics governing vibratory pollen release and establish a foundation for future work exploring artificial pollination techniques and ecological implications.

Limitations

While this study provides valuable insights into pollen expulsion dynamics, several limitations must be acknowledged. These limitations stem from necessary model assumptions, computational constraints, and the simplifications used to isolate specific physical effects. Addressing these challenges will be essential for refining future models and improving our understanding of vibratory pollen expulsion.

Simplified Representation of Pollen Grain Interactions

The discrete element method model used in this study assumes simplified pollen grain interactions, primarily focusing on elastic collisions without fully incorporating detailed surface adhesion forces. In reality, pollen grains exhibit complex interactions influenced by electrostatic forces, van der Waals interactions, and surface roughness. While the Hertz-Mindlin contact model accounts for elastic deformations and damping effects, it does not fully capture these adhesion forces, which may play a role in real anther environments.

Idealized Vibration Conditions

The simulations implemented controlled sinusoidal excitation at discrete frequencies and amplitudes. However, real pollinators exhibit variations in buzzing frequencies, amplitudes, and excitation profiles. The assumption of periodic excitation simplifies the analysis but does not fully capture the variability observed in natural buzz pollination events. Additionally, real anthers may not behave as perfectly rigid or flexible structures, potentially affecting pollen expulsion dynamics.

Assumptions in Translating Anther Simulations

The translating anther simulations assumed a rigid, non-deforming structure undergoing uniform motion. While this approach effectively isolated granular dynamics, it did not

account for how real anthers flex and deform under vibrational loading. In reality, anther deformation could create additional force fluctuations that influence pollen expulsion trends.

Challenges in Deforming Anther Simulations

The deforming anther simulations were computationally expensive, limiting the number of parameter sets explored in this study. While the first and second mode shapes were investigated, other deformation modes could also contribute significantly to pollen ejection. Additionally, the prescribed modal vibrations assume idealized boundary conditions, whereas real anthers may exhibit complex anchoring points and damping properties that alter vibration behavior.

Material Property Assumptions

The material properties of both pollen grains and anther walls were estimated based on previous studies, but the true mechanical behavior of these biological materials remains uncertain. Hydration levels, surface composition, and microscopic deformations could all influence pollen expulsion, yet these effects were not explicitly modeled.

Computational Constraints

Despite the advantages of DEM for modeling granular interactions, computational constraints limited the number of pollen grains simulated and the duration of simulations. The reduced number of simulated pollen grains compared to real anthers may affect bulk behavior trends. Additionally, while simulations captured major expulsion trends, extending the simulation time could provide further insights into long-term pollen transport dynamics. An initial study of the translating model between 10,000 and 100,000 particles showed only a minor change in $\dot{P}$, this should be repeated across different simulation setups to ensure proper convergence is maintained.

The Role of Restitution in Pollen Expulsion

The simulations investigated how different restitution coefficients affect expulsion rates, showing that lower restitution values proportionally reduced the rate of expulsion. While this provides insight into the role of particle elasticity in pollen expulsion, real anthers introduce additional complexities such as hydration-dependent stiffness and surface adhesion effects. The precise impact of material damping on pollen expulsion in natural systems remains an open question.

Experimental Validation Challenges

While DEM provides a robust framework for studying pollen expulsion mechanics, experimental validation is necessary to confirm key findings. Many aspects of pollen motion remain difficult to observe directly due to the opacity of anthers and the high-speed nature of buzz pollination.

Future Work

Addressing these limitations presents several directions for future research. Incorporating additional physical effects, refining model assumptions, and integrating experimental validation techniques will be crucial to improving our understanding of pollen expulsion mechanics.

Incorporating Adhesion and Triboelectric Effects

Future DEM simulations should incorporate adhesion and triboelectric charging to provide a more realistic representation of pollen interactions. Investigating how pollen charge distributions and adhesion properties influence expulsion efficiency could yield insights into real anther environments.

Using Experimentally Recorded Buzzing Profiles

Future research should incorporate experimentally recorded pollination buzzes as input waveforms for simulations instead of relying solely on sinusoidal excitations. This would provide a more accurate representation of how pollinator-induced variability influences pollen expulsion.

Modeling Flexible Anthers

Incorporating flexible anther models in future simulations could help assess the role of structural deformation in pollen release. A coupled structural-pollen interaction model could provide a more accurate representation of how energy is transferred between anther walls and pollen grains.

Expanding Deforming Anther Simulations

Expanding the parameter space for deforming anther simulations and incorporating experimentally derived anther deformation profiles would provide a more comprehensive understanding of how structural vibrations influence pollen expulsion. Analyzing additional mode shapes and their corresponding force distributions could refine the role of deformation in pollen expulsion efficiency.

Improving Pollen Material Property Data

Experimental validation of pollen mechanical properties is necessary to refine simulation inputs. Techniques such as atomic force microscopy (AFM) could provide direct measurements of pollen stiffness, adhesion forces, and deformation characteristics.

Enhancing Computational Performance

Future studies could explore high-performance computing (HPC) approaches to enable larger-scale simulations that better approximate real anther-pollen systems. GPU-

accelerated DEM solvers or parallelized computing techniques could significantly improve the resolution and realism of pollen expulsion modeling.

Integrating Experimental Validation Through PIV

A promising avenue for validation is the use of Particle Image Velocimetry (PIV), which is currently being explored at Montana State University. PIV can track expelled pollen motion under controlled vibratory excitation, allowing for a comparison between simulated and experimental pollen dispersal patterns. While PIV does not directly inform DEM model inputs, it provides a benchmark for validating pollen expulsion trajectories, velocity distributions, and clustering behavior.

Future comparisons between PIV-derived pollen ejection data and DEM simulations could reveal discrepancies in dispersal trends and provide insight into model refinements. If differences arise, adjustments to particle-particle interaction models, restitution coefficients, or adhesion effects could be explored to improve simulation accuracy. Additionally, PIV can provide quantitative measurements of pollen cloud dispersion, offering insight into the post-expulsion transport of pollen grains.

Developing Integrated Pollination Models

Future studies should aim to integrate pollen expulsion models with broader ecological and reproductive success metrics. Understanding how mechanical pollen expulsion translates to successful pollination would provide a more comprehensive picture of the role of buzz pollination in plant reproduction.

Summary of Future Directions

Addressing these challenges will require a combination of computational advancements and experimental validation. Future work should focus on incorporating additional physical effects, refining model assumptions, and integrating real-world data into numerical

simulations. By bridging the gap between computational modeling and experimental observations, future research can provide deeper insights into the biomechanical principles underlying buzz pollination.

Final Remarks and Broader Implications

This study provides a novel computational approach to understanding pollen expulsion in buzz-pollinated anthers, offering key insights into how vibration parameters, granular interactions, and anther deformation influence pollen release. By identifying the role of jerk as a governing parameter in translating anther simulations and demonstrating the significance of inter-particle interactions, this work advances the biomechanical framework for vibratory pollen ejection.

Deforming anther simulations extended this framework by demonstrating how spatially complex deformation patterns further influence pollen expulsion dynamics. These simulations demonstrated that modal deformation not only affects interaction mechanisms and temporal dynamics but also introduces complexities that challenge the direct application of parameters, such as jerk. The spatial variability inherent in deforming anthers underscores the need for developing new parameters or frameworks capable of capturing both temporal and spatial deformation effects in pollen expulsion models.

Beyond its fundamental contributions, this research has practical implications for artificial pollination technologies, where optimizing vibration profiles could enhance pollen extraction efficiency in agricultural settings. The findings also highlight the need for experimental validation to refine model predictions and better understand how real anthers respond to vibratory excitation.

Moving forward, integrating high-resolution experimental techniques with computational modeling will be essential for bridging the gap between simulation-based insights and real-world pollination mechanics. By continuing to refine our understanding of

pollen expulsion dynamics, particularly through incorporating spatial complexity into predictive models, future research can contribute to both conservation efforts and agricultural innovation, ensuring the continued success of pollination-dependent ecosystems.

REFERENCES CITED

[1] Marcelo A. Aizen, Lucas A. Garibaldi, Saul A. Cunningham, and Alexandra M. Klein. How much does agriculture depend on pollinators? Lessons from long-term trends in crop production. *Annals of Botany*, 103(9):1579–1588, June 2009. ISSN 1095-8290. doi: 10.1093/aob/mcp076.

[2] Alexandra-Maria Klein, Bernard E. Vaissière, James H. Cane, Ingolf Steffan-Dewenter, Saul A. Cunningham, Claire Kremen, and Teja Tscharntke. Importance of pollinators in changing landscapes for world crops. *Proceedings of the Royal Society B: Biological Sciences*, 274:303–313, October 2006. doi: https://doi.org/10.1098/rspb.2006.3721. URL `https://royalsocietypublishing.org/doi/10.1098/rspb.2006.3721`.

[3] George E. Bowker and Hugh C. Crenshaw. Electrostatic forces in wind-pollination-Part 1: Measurement of the electrostatic charge on pollen. *Atmospheric Environment*, 41(8): 1587–1595, 3 2007. ISSN 13522310. doi: 10.1016/j.atmosenv.2006.10.047.

[4] Anže Božič and Antonio Šiber. Mechanical design of apertures and the infolding of pollen grain. *The Proceedings of the National Academy of Sciences*, 117:26600–26607, 2020. doi: 10.1073/pnas.2011084117/-/DCSupplemental.y. URL `www.pnas.org/cgi/doi/10.1073/pnas.2011084117`.

[5] Stephen Buchmann. Buzz Pollination in Angiosperms. In *Handbook of Experimental Pollination Biology*, pages 73–113. Van Nostrand Reinhold Company Inc., New York, NY, USA, 1983. ISBN 0-442-24676-5.

[6] Stephen L Buchmann. Bees Use Vibration to Aid Pollen Collection from Non-Poricidal Flowers. *Journal of the Kansas Entomological Society*, 58(3):517–525, 1985. URL `https://www.jstor.org/stable/25084671`.

[7] Stephen L Buchmann and James P Hurley. A Biophysical Model for Buzz Pollination in Angiosperms. *Journal of Theoretical Biology*, 72(4):639–657, 1978. ISSN 0022-5193.

[8] Hazel Cooley and Mario Vallejo-Marín. Buzz-Pollinated Crops: A Global Review and Meta-analysis of the Effects of Supplemental Bee Pollination in Tomato. *Journal of Economic Entomology*, 114(2):505–519, April 2021. ISSN 0022-0493. doi: 10.1093/jee/toab009. URL `https://doi.org/10.1093/jee/toab009`.

[9] Sarah A. Corbet and Shuang-Quan Huang. Buzz pollination in eight bumblebee-pollinated *pedicularis* species: does it involve vibration-induced triboelectric charging of pollen grains? *Annals of Botany*, 114(8):1665–1674, Dec 2014. doi: 10.1093/aob/mcu195. URL `https://doi.org/10.1093/aob/mcu195`.

[10] P. A. Cundall and O. D. L. Strack. A discrete numerical model for granular assemblies. *Géotechnique*, 29(1):47–65, March 1979. ISSN 0016-8505. doi: 10.1680/geot.1979.29.1.47. URL `https://www.icevirtuallibrary.com/doi/10.1680/geot.1979.29.1.47`.

[11] P.A. De Luca, L.F. Bussière, D. Souto-Vilaros, and Mario Vallejo-Marín. Variability in bumblebee pollination buzzes affects the quantity of pollen released from flowers. *Oecologia*, 172:805–816, 2013. doi: 10.1007/s00442-012-2535-1. URL https://doi.org/10.1007/s00442-012-2535-1.

[12] Alberto Di Renzo and Francesco Paolo Di Maio. Comparison of contact-force models for the simulation of collisions in DEM-based granular flow codes. *Chemical Engineering Science*, 59(3):525–541, February 2004. ISSN 0009-2509. doi: 10.1016/j.ces.2003.09.037. URL https://www.sciencedirect.com/science/article/pii/S0009250903005414.

[13] Matheus Hansen, Gabriel C. Lanes, Vinícius L.G. Brito, and Edson D. Leonel. Investigation of pollen release by poricidal anthers using mathematical billiards. *Physical Review E*, 104(3):034409, 9 2021. ISSN 24700053. doi: 10.1103/PhysRevE.104.034409.

[14] L. D. Harder and R. M. R. Barclay. The functional significance of poricidal anthers and buzz pollination: Controlled pollen removal from dodecatheon. *Functional Ecology*, 8 (4):509–517, 1994. ISSN 02698463, 13652435. URL http://www.jstor.org/stable/2390076.

[15] Lawrence D. Harder and James D. Thomson. Evolutionary options for maximizing pollen dispersal of animal-pollinated plants. *The American Naturalist*, 133(3):323–344, 1989. doi: 10.1086/284926. URL https://doi.org/10.1086/284926.

[16] N. Inari, S. Suzuki, K. Okabe, and H. Tanaka. Non-compliance with the world trade organization agreements by countries banning bumblebee imports. *Journal of Environmental Policy and Trade*, 15(2):245–261, 2023. doi: 10.1080/15487733.2023.2256173. URL https://www.tandfonline.com/doi/full/10.1080/15487733.2023.2256173.

[17] Mark Jankauski, Riggs Ferguson, Avery Russell, and Stephen Buchmann. Structural dynamics of real and modelled *Solanum* stamens: implications for pollen ejection by buzzing bees. *Journal of The Royal Society Interface*, 19(188):20220040, 03 2022. doi: 10.1098/rsif.2022.0040.

[18] Jurene E. Kemp and Mario Vallejo-Marín. Pollen dispensing schedules in buzz-pollinated plants: experimental comparison of species with contrasting floral morphologies. *American Journal of Botany*, 108(6):993–1005, 2021. doi: 10.1002/ajb2.1680.

[19] Jeremy T. Kerr et al. Climate change impacts on bumblebees converge across continents. *Science*, 349(6244):177–180, 2015. doi: 10.1126/science.aaa7031. URL https://www.science.org/doi/10.1126/science.aaa7031.

[20] M. J. King and S. L. Buchmann. Sonication dispensing of pollen from solanum laciniatum flowers. *Functional Ecology*, 10(4):449–456, 1996. ISSN 02698463, 13652435. URL http://www.jstor.org/stable/2389937.

[21] Pushpa Karna Mallick. Pollen Grains Morphology of Angiosperms. *International Journal of Applied Sciences and Biotechnology*, 8(2):205–210, 6 2020. doi: 10.3126/ijasbt.v8i2.28520.

[22] Lucy Nevard and Mario Vallejo-Marín. Floral orientation affects outcross-pollen deposition in buzz-pollinated flowers with bilateral symmetry. *American Journal of Botany*, 109(10):1568–1578, 2022. doi: 10.1002/ajb2.16078.

[23] Marine J. Paupière, Yury M. Tikunov, Nurit Firon, Ric C.H. de Vos, Chris Maliepaard, Richard G.F. Visser, and Arnaud G. Bovy. The effect of isolation methods of tomato pollen on the results of metabolic profiling. *Metabolomics*, 15(11), 1 2019. ISSN 15733890. doi: 10.1007/s11306-018-1471-4.

[24] Simon G. Potts, Vera Imperatriz-Fonseca, Hien T. Ngo, Marcelo A. Aizen, Jacobus C. Biesmeijer, Thomas D. Breeze, Lynn V. Dicks, Lucas A. Garibaldi, Rosemary Hill, Josef Settele, and Adam J. Vanbergen. Safeguarding pollinators and their values to human well-being. *Nature*, 540(7632):220–229, December 2016. ISSN 1476-4687. doi: 10.1038/nature20588. URL `https://www.nature.com/articles/nature20588`.

[25] Zihao Qu and J. Carson Meredith. The atypically high modulus of pollen exine. *Journal of the Royal Society Interface*, 15(146):20180533, 9 2018. ISSN 17425662. doi: 10.1098/rsif.2018.0533.

[26] B. Reade, P. Croxford, T. Nishimura, and J. Shorter. Csr, biodiversity and japan's stakeholder approach to the global bumble bee trade. *International Review of Environmental Law*, 26(4):587–608, 2014. URL `https://www.researchgate.net/publication/269765008_CSR_Biodiversity_and_Japan%27s_Stakeholder_Approach_to_the_Global_Bumble_Bee_Trade`.

[27] Conrado Augusto Rosi-Denadai, Priscila Cássia Souza Araújo, Lucio Antônio de Oliveira Campos, Lirio Cosme, and Raul Narciso Carvalho Guedes. Buzz-pollination in Neotropical bees: genus-dependent frequencies and lack of optimal frequency for pollen release. *Insect Science*, 27(1):133–142, 2 2020. ISSN 17447917. doi: 10.1111/1744-7917.12602.

[28] Avery L. Russell, Stephen L. Buchmann, John S. Ascher, Zhiheng Wang, Ricardo Kriebel, Diana D. Jolles, Michael C. Orr, and Alice C. Hughes. Global patterns and drivers of buzzing bees and poricidal plants. *Current Biology*, 34:3055–3063, 2024. doi: 10.1016/j.cub.2024.05.065.

[29] Harry Siviter et al. Toxic temperatures: Bee behaviours exhibit divergent pesticide sensitivity. *Functional Ecology*, 35(6):1284–1296, 2021. doi: 10.1111/1365-2435.13818. URL `https://pubmed.ncbi.nlm.nih.gov/36944569/`.

[30] Siemens Digital Industries Software. Simcenter STAR-CCM+ User Guide, version 2206. In *Discrete Element Method (DEM)*. Siemens, 2022.

[31] L. M. Sosnoskie, T. M. Webster, D. Dales, G. C. Rains, T. L. Grey, and A. S. Culpepper. Pollen grain size, density, and settling velocity for palmer amaranth (amaranthus palmeri). *Weed Science*, 57(4):404–409, 2009. doi: 10.1614/WS-08-157.1.

[32] Francisco Sánchez-Bayo and Kris A. G. Wyckhuys. Worldwide decline of the entomofauna: A review of its drivers. *Biological Conservation*, 232:8–27, 2019. doi: 10.1016/j.biocon.2019.01.020. URL `https://doi.org/10.1016/j.biocon.2019.01.020`.

[33] Herwig Teppner. The first records of vibratory pollen-collection by bees. *Phyton-International Journal of Experimental Botany*, 57(1-2):129–135, 2018. doi: 10.12905/0380.phyton57-2018-0129.

[34] Y. Tsuji, T. Tanaka, and T. Ishida. Lagrangian numerical simulation of plug flow of cohesionless particles in a horizontal pipe. *Powder Technology*, 71(3):239–250, September 1992. ISSN 0032-5910. doi: 10.1016/0032-5910(92)88030-L. URL `https://www.sciencedirect.com/science/article/pii/003259109288030L`.

[35] Mario Vallejo-Marín. Buzz pollination: studying bee vibrations on flowers. *New Phytologist*, 224(3):1068–1074, 11 2019. ISSN 14698137. doi: 10.1111/nph.15666.

[36] Mario Vallejo-Marín, Catriona Walker, Philip Friston-Reilly, Lislie Solís-Montero, and Boris Igic. Recurrent modification of floral morphology in heterantherous solanum reveals a parallel shift in reproductive strategy. *Philosophical Transactions of the Royal Society B: Biological Sciences*, 369:20130256, 2014. doi: 10.1098/rstb.2013.0256. URL `http://doi.org/10.1098/rstb.2013.0256`.

[37] R. van Hout and J. Katz. A method for measuring the density of irregularly shaped biological aerosols such as pollen. *Journal of Aerosol Science*, 35(11):1369–1384, 2004. ISSN 0021-8502. doi: https://doi.org/10.1016/j.jaerosci.2004.05.008. URL `https://www.sciencedirect.com/science/article/pii/S0021850204000928`.

[38] Rachael Winfree et al. A meta-analysis of bees' responses to anthropogenic disturbance. *Ecology*, 90(8):2068–2076, 2009. doi: 10.1890/08-1245.1. URL `https://esajournals.onlinelibrary.wiley.com/doi/10.1890/08-1245.1`.